R. & M. No. 3241

MINISTRY OF AVIATION

AERONAUTICAL RESEARCH COUNCIL
REPORTS AND MEMORANDA

An Approximate Integral Method for Calculating the Incompressible Laminar Boundary Layer on an Infinite Swept Wing on which Velocity and Suction Distribution are Arbitrary

By H. G. and P. A. PINSENT

LONDON: HER MAJESTY'S STATIONERY OFFICE
1962
PRICE: 15*s.* 0*d.* NET

An Approximate Integral Method for Calculating the Incompressible Laminar Boundary Layer on an Infinite Swept Wing on which Velocity and Suction Distribution are Arbitrary

By H. G. and P. A. PINSENT

*Reports and Memoranda No. 3241**

February, 1959

Summary. The method described in this Report gives an approximate solution for the cross-flow velocity in an incompressible laminar boundary layer on an infinite swept wing. The cross flow is defined as that velocity in the boundary layer in a direction normal to the outer flow streamline. The two-dimensional flow in the chordwise direction is assumed known.

The boundary-layer equations are expressed in a non-dimensional form. Head's method, which is based on the momentum and energy equations and is used to solve the two-dimensional flow, is briefly described. From the non-dimensional boundary-layer equations, an equation involving the cross-flow profile directly is obtained. This equation is then integrated throughout the boundary layer giving two integral equations. Typical cross-flow shapes have been used to calculate functions which when used in conjunction with the two integral equations and the boundary condition at the wall enable the cross flow to be determined for arbitrary velocity and suction distributions. The stability criterion for three-dimensional flow is expressed in the notation of this method and is a simple condition on the cross flow.

The method is then applied to the upper and lower surfaces of a wing, suction distributions being calculated to maintain stability at each point of the wing. For the lower surface comparison is made with an independent method (Ref. 1) in the adverse pressure-gradient region.

Two more sets of comparisons are made, each with an exact solution. The method is tested on a number of similar solutions, and on an exact solution obtained by American workers (Ref. 8). Consideration is also given to some difficulties encountered in the use of the method.

* Previously issued as Handley Page Research Report No. 54—A.R.C. 22,154.

1. *The Cross Flow.*

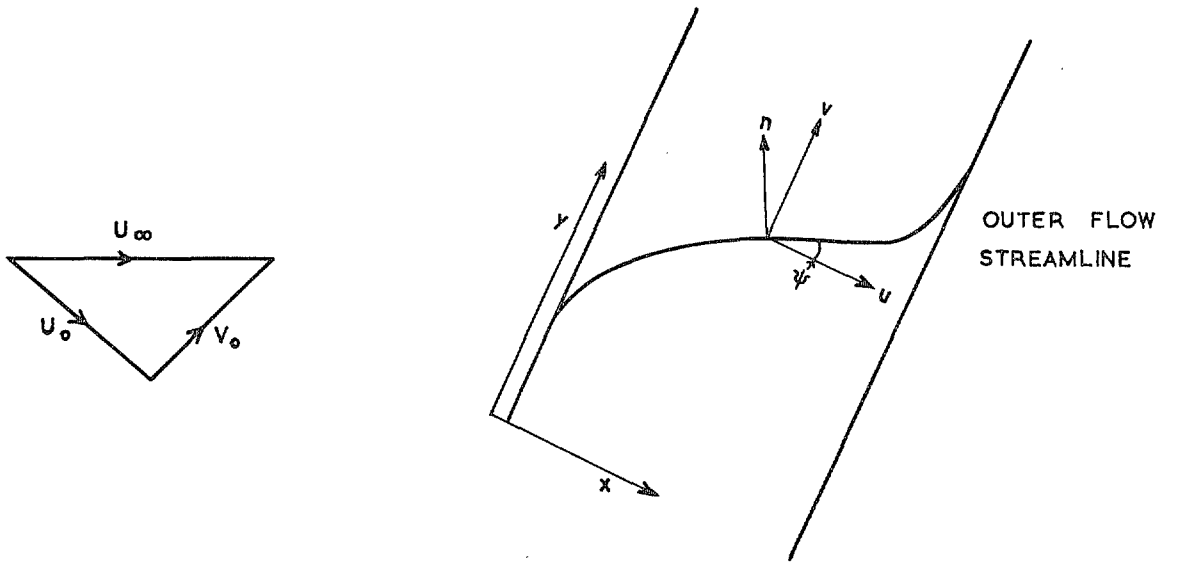

(i)

In Fig. (i), U_0 and V_0 are the components of the free-stream velocity U_∞, in the chordwise and spanwise directions respectively. Within the boundary layer on the infinite swept wing, the components are u and v, becoming $U(x)$ and a constant V_0, outside the boundary layer. The cross flow n is defined as that velocity in the boundary layer in the direction normal to the outer flow streamline, *i.e.*, from Fig. (i)

$$n = v\cos\psi - u\sin\psi$$

$$= \frac{v}{V_0}V_0\cos\psi - \frac{u}{U}U\sin\psi,$$

but

$$V_0\cos\psi = U\sin\psi = \frac{UV_0}{(U^2+V_0^2)^{1/2}}.$$

therefore

$$n = \frac{UV_0}{(U^2+V_0^2)^{1/2}}\left(\frac{v}{V_0}-\frac{u}{U}\right) = \frac{U_0\bar{U}\bar{V}}{(\bar{U}^2+\bar{V}^2)^{1/2}}\left(\frac{v}{V_0}-\frac{u}{U}\right),$$

where

$$\bar{U} = \frac{U}{U_0} \text{ and } \bar{V} = \frac{V_0}{U_0}.$$

It is thus seen that n, the cross flow, is directly proportional to the difference of the velocity profiles in the chordwise and spanwise directions, which is denoted by N, the cross-flow profile.

2. *The Boundary-Layer Equations.* 2.1. The boundary-layer equations on an infinite wing are (derivatives with respect to y being zero)

Chordwise:

$$u\frac{\partial u}{\partial x} + w\frac{\partial u}{\partial z} = U\frac{dU}{dx} + \nu\frac{\partial^2 u}{\partial z^2}. \tag{1}$$

Spanwise:

$$u\frac{\partial v}{\partial x} + w\frac{\partial v}{\partial z} = \nu\frac{\partial^2 v}{\partial z^2}. \tag{2}$$

Continuity:

$$\frac{\partial u}{\partial x} + \frac{\partial w}{\partial z} = 0, \text{ i.e., } w = w_0 - \int_0^z \frac{\partial u}{\partial x}\,dz. \tag{3}$$

Using the variables

$$X = \frac{x}{c_0}, \qquad Z = \frac{z}{c_0}\frac{R_c^{1/2}}{\sqrt{t^*}}, \qquad T = \frac{u}{U}, \qquad S = \frac{v}{V},$$

where

$$R_c = \frac{U_0 c_0}{\nu}, \qquad t^*(X) = \left(\frac{\theta}{c_0}\right)^2 \frac{U_0 c_0}{\nu},$$

θ being the momentum thickness, *i.e.*, $\theta = \int_0^\infty T(1-T)dz$.

The boundary-layer equations become, in non-dimensional form

$$\bar{U}T\frac{\partial T}{\partial X} + \frac{\partial T}{\partial Z}\left[\frac{W_0}{\sqrt{t^*}} - \int_0^z \frac{\partial}{\partial X}(\bar{U}T)dZ - \tfrac{1}{2}\frac{t^{*\prime}}{t^*}\int_0^z \bar{U}T\,dZ\right]$$

$$= \frac{1}{t^*}\frac{\partial^2 T}{\partial Z^2} + (1-T^2)\bar{U}', \tag{4}$$

$$\bar{U}T\frac{\partial S}{\partial X} + \frac{\partial S}{\partial Z}\left[\frac{W_0}{\sqrt{t^*}} - \int_0^z \frac{\partial}{\partial X}(\bar{U}T)dZ - \tfrac{1}{2}\frac{t^{*\prime}}{t^*}\int_0^z \bar{U}T\,dZ\right]$$

$$= \frac{1}{t^*}\frac{\partial^2 S}{\partial Z^2}, \tag{5}$$

where dashes denote total differentiation with respect to X.

2.2. The familiar chordwise momentum and energy equations can be derived by multiplying Equation (4) throughout by factors 1 and $T(X, Z)$ and integrating the variable Z from the boundary wall to infinity. In his method of solving the two dimensional flow, Dr. M. R. Head (Ref. 2), has considered a two-parameter system of profiles denoted by $T = T(Z, l(X), m(X))$ where the parameters l and m are the first and second derivatives of T at the wall, *i.e.*,

$$l = \left(\frac{\partial T}{\partial Z}\right)_{Z=0}, \qquad m = \left(\frac{\partial^2 T}{\partial Z^2}\right)_{Z=0}.$$

Defining the functions

$$H(l, m) = \int_0^\infty (1 - T)dZ$$

$$H_c(l, m) = \int_0^\infty T(1 - T^2)dZ$$

$$D^*(l, m) = \int_0^\infty \left(\frac{\partial T}{\partial Z}\right)^2 dZ$$

and writing

$$\Lambda = \bar{U}'t^*, \qquad \lambda = -\frac{w_0}{U_0}\sqrt{t^*}\sqrt{\left(\frac{U_0 c}{\nu}\right)}$$

$$= -W_0\sqrt{t^*},$$

the momentum and energy equations become

$$t^{*\prime} = \frac{2}{\bar{U}}(l - \Lambda(H+2) - \lambda), \tag{6}$$

$$H_c' = \frac{1}{\bar{U}t^*}[2D^* - H_c\{l - \Lambda(H-1) - \lambda\} - \lambda]. \tag{7}$$

From Equation (4) the boundary condition at the wall becomes

$$m = -\Lambda - l\lambda. \tag{8}$$

Dr. Head gives a step-by-step process by which these three equations may be solved for the three unknowns t^*, l, m, using charts for H, H_c and $2D^*$ as functions of l and m. A numerical form of these charts, used in the present calculations, may be found in Appendix I, with the equations suitably adapted.

The T profile itself can be obtained from charts published in Ref. 2.

2.3. By subtracting Equation (4) from Equation (5) the following equation is derived for the cross-flow profile $N = S - T$.

$$\bar{U}T\frac{\partial N}{\partial X} + \frac{\partial N}{\partial Z}\left[\frac{W_0}{\sqrt{t^*}} - \int_0^z \frac{\partial}{\partial X}(\bar{U}T)dZ - \tfrac{1}{2}\frac{t^{*\prime}}{t^*}\int_0^z \bar{U}T dZ\right]$$

$$= \frac{1}{t^*}\frac{\partial^2 N}{\partial Z^2} - (1 - T^2)\bar{U}'. \tag{9}$$

Since N is in general small compared with unity, it is preferable to deal with this equation directly rather than the spanwise equation, to solve the three-dimensional component of the boundary layer.

The cross-flow Equation (9) is now dealt with in integrated form. Multiplying both sides by $j(N, T)$ and integrating the variable Z from the boundary wall, *i.e.*, $Z = 0$, through the boundary layer, the equation becomes

$$\int_0^\infty \bar{U}T\frac{\partial N}{\partial X}j(N, T)dZ + \int_0^\infty \frac{\partial N}{\partial Z}j(N, T)\left[\frac{W_0}{\sqrt{t^*}} - \int_0^z \frac{\partial}{\partial X}(\bar{U}T)dZ - \tfrac{1}{2}\frac{t^{*\prime}}{t^*}\int_0^z \bar{U}T dZ\right]dZ$$

$$= \frac{1}{t^*}\int_0^\infty j(N, T)\frac{\partial^2 N}{\partial Z^2}dZ - \bar{U}'\int_0^\infty (1 - T^2)j(N, T)dZ. \tag{10}$$

In the left-hand side of Equation (10) $\int_0^\infty \bar{U}T\frac{\partial N}{\partial \bar{X}}jdZ$ may be replaced by

$$\bar{U}\frac{\partial}{\partial \bar{X}}\int_0^\infty TNjdZ - \bar{U}\int_0^\infty N\frac{\partial T}{\partial \bar{X}}jdZ - \bar{U}\int_0^\infty NT\frac{\partial j}{\partial \bar{X}}dZ$$

and the remaining term may be integrated by parts, giving

$$\left[Nj\left(\frac{W_0}{\sqrt{t^*}} - \int_0^z \frac{\partial}{\partial \bar{X}}(\bar{U}T)dZ - \tfrac{1}{2}\frac{t^{*\prime}}{t^*}\int_0^z \bar{U}TdZ\right)\right]_0^\infty -$$

$$-\int_0^\infty N\left[j\left\{-\frac{\partial}{\partial \bar{X}}(\bar{U}T) - \tfrac{1}{2}\frac{t^{*\prime}}{t^*}\bar{U}T\right\} +\right.$$

$$\left.+\frac{\partial j}{\partial Z}\left\{\frac{W_0}{\sqrt{t^*}} - \int_0^z \frac{\partial}{\partial \bar{X}}(\bar{U}T)dZ - \tfrac{1}{2}\frac{t^{*\prime}}{t^*}\int_0^z \bar{U}TdZ\right\}\right]dZ.$$

The term to be evaluated between zero and infinity may be taken as zero since $N = 0$ both at $Z = 0$ and as $Z \to \infty$ and j is taken to be bounded.
Using the relations

$$\frac{\partial j}{\partial \bar{X}} = \left(\frac{\partial j}{\partial N}\right)_T\frac{\partial N}{\partial \bar{X}} + \left(\frac{\partial j}{\partial T}\right)_N\frac{\partial T}{\partial \bar{X}}$$

and

$$\frac{\partial j}{\partial Z} = \left(\frac{\partial j}{\partial N}\right)_T\frac{\partial N}{\partial Z} + \left(\frac{\partial j}{\partial T}\right)_N\frac{\partial T}{\partial Z}$$

the left-hand side becomes,

$$\bar{U}\frac{\partial}{\partial \bar{X}}\int_0^\infty TNjdZ + \left(\bar{U}' + \tfrac{1}{2}\frac{t^{*\prime}}{t^*}\bar{U}\right)\int_0^\infty TNjdZ -$$

$$-\int_0^\infty N\left[\frac{\partial j}{\partial N}\left\{\bar{U}T\frac{\partial N}{\partial \bar{X}} + \left[\frac{W_0}{\sqrt{t^*}} - \int_0^z \frac{\partial}{\partial \bar{X}}(\bar{U}T)dZ - \tfrac{1}{2}\frac{t^{*\prime}}{t^*}\int_0^z \bar{U}TdZ\right]\frac{\partial N}{\partial Z}\right\} +\right.$$

$$\left.+\frac{\partial j}{\partial T}\left\{\bar{U}T\frac{\partial T}{\partial \bar{X}} + \left[\frac{W_0}{\sqrt{t^*}} - \int_0^z \frac{\partial}{\partial \bar{X}}(\bar{U}T)dZ - \tfrac{1}{2}\frac{t^{*\prime}}{t^*}\int_0^z \bar{U}TdZ\right]\frac{\partial T}{\partial Z}\right\}\right]dZ.$$

Substituting the left-hand side of each of Equations (4) and (9) into the expression above, the following general integral equation is finally obtained,

$$\bar{U}\frac{\partial}{\partial \bar{X}}\int_0^\infty TNjdZ + \left(\bar{U}' + \tfrac{1}{2}\frac{t^{*\prime}}{t^*}\bar{U}\right)\int_0^\infty TNjdZ -$$

$$-\int_0^\infty N\left[\frac{\partial j}{\partial N}\left\{\frac{1}{t^*}\frac{\partial^2 N}{\partial Z^2} - (1-T^2)\bar{U}'\right\} + \frac{\partial j}{\partial T}\left\{\frac{1}{t^*}\frac{\partial^2 T}{\partial Z^2} + (1-T^2)\bar{U}'\right\}\right]dZ$$

$$= \frac{1}{t^*}\int_0^\infty j\frac{\partial^2 N}{\partial Z^2}dZ - \bar{U}'\int_0^\infty (1-T^2)jdZ. \qquad (11)$$

2.4. By choosing $j(T, N)$ equal to 1 and $1 - T$, two integral equations linear in N are obtained. Defining

$$r_1 = \int_0^\infty NTdZ$$

$$r_2 = \int_0^\infty NT(1-T)dZ$$

$$s_1 = \int_0^\infty N(1-T)dZ$$

$$s_2 = \int_0^\infty \frac{\partial N}{\partial Z}\frac{\partial T}{\partial Z}dZ$$

$$s_3 = \left(\frac{\partial N}{\partial Z}\right)_{Z=0}$$

$$s_4 = -\left(\frac{\partial^2 N}{\partial Z^2}\right)_{Z=0},$$

these two equations become

$$r_1' = \frac{-1}{\bar{U}t^*}\left[r_1(\Lambda + \tfrac{1}{2}\bar{U}t^{*\prime}) + \Lambda(1+H) + s_3\right] \tag{12}$$

$$r_2' = \frac{-1}{\bar{U}t^*}\left[r_2(2\Lambda + \tfrac{1}{2}\bar{U}t^{*\prime}) + \Lambda(1+H-H_e) + s_3 - 2s_2 + \Lambda s_1\right] \tag{13}$$

the boundary condition at the wall, from Equation (9) being

$$s_3\lambda = s_4 + \Lambda. \tag{14}$$

Since there are three equations, N can be chosen to depend on three arbitrary parameters. Given these parameters, the cross-flow profile is known.
Let

$$N = \begin{cases} af(\eta) + by(\eta) \text{ for } 0 \leqslant \eta \leqslant 1 \\ 0 \text{ for } \eta > 1, \text{ where } \eta = \dfrac{Z}{10\sigma}. \end{cases} \tag{15}$$

($f(\eta)$ and $g(\eta)$ are typical profile shapes which will be dealt with in Section 3).
a and b are scaling parameters giving the magnitude of the N profile, their ratio determining its shape. σ is a parameter which gives the thickness of the N profile with respect to the chordwise boundary layer.

Using the definition (15) it can be seen that $r_1 = \int_0^\infty NTdZ$ and $r_2 = \int_0^\infty NT(1-T)dZ$ may be obtained as linear functions of a and b with coefficients which will depend on the parameters σ, l, m. It therefore follows that a and b can be written in the form

$$\begin{aligned} a &= -r_1\alpha_1(\sigma, l, m) + r_2\alpha_2(\sigma, l, m) \\ b &= -r_1\beta_1(\sigma, l, m) + r_2\beta_2(\sigma, l, m), \end{aligned} \tag{16}$$

where it is supposed that α_1, α_2, β_1 and β_2 are known as functions of σ, l and m.

Also

$$s_3 = \frac{1}{10\sigma}\left[a\left(\frac{df}{d\eta}\right)_{\eta=0} + b\left(\frac{dg}{d\eta}\right)_{\eta=0}\right]$$

$$s_4 = \frac{-1}{100\sigma^2}\left[a\left(\frac{d^2f}{d\eta^2}\right)_{\eta=0} + b\left(\frac{d^2g}{d\eta^2}\right)_{\eta=0}\right],$$

the derivatives being known constants.

Defining $E = \lambda s_3 - s_4 - \Lambda$ the boundary condition is satisfied when $E = 0$.

A step-by-step method can be used in the solution.

At the beginning of a typical step, all quantities on the right-hand side of Equations (12) and (13) are known. The values of the derivatives r_1' and r_2' may, therefore, be calculated and hence r_1 and r_2 at the end of the step derived.

The chordwise solution is known at the end of the step, hence values of l, m, λ and Λ are given.

Taking suitable values of σ, coefficients α_1, α_2, β_1, β_2 can be found and hence using the values of r_1 and r_2, a and b can be calculated for each value of σ, and thus s_3 and s_4, and E can be found for each σ. Cross plotting E against σ to find the value of σ satisfying the boundary condition, the values of a, b, s_3 and s_4 can be derived and hence the N profile is determined. Finally it is possible to complete the step by obtaining s_1 and s_2 from the definitions

$$s_1 = \int_0^\infty N(1-T)dZ = a10\sigma\int_0^1 f(\eta)d\eta + b10\sigma\int_0^1 g(\eta)d\eta - r_1$$

$$s_2 = \int_0^\infty \frac{\partial N}{\partial Z}\frac{\partial T}{\partial Z} = -r_1 d_1(\sigma, l, m) + r_2 d_2(\sigma, l, m),$$

where d_1 and d_2 may be obtained for values of l, m, and σ.

In practice it has been found to be quicker to keep plots of the quantities r_1, r_2, s_1, s_2, s_3 against X and thus to find the extrapolated values at the middle of the step. The derivatives r_1' and r_2' can thus be calculated and r_1 and r_2 at the end of the step obtained. If these are inconsistent with the extrapolated r_1 and r_2, it is a simple matter to repeat this process to obtain consistency. Since all the quantities r_1, r_2, s_1, s_2, s_3, are linear in N (note that

$$s_2 = \int_0^\infty \frac{\partial N}{\partial Z}\frac{\partial T}{\partial Z}dZ = -\int_0^\infty N\frac{\partial^2 T}{\partial Z^2}dZ)$$

their plots are similar in shape which is helpful in the process of extrapolation. Using the values of r_1 and r_2 and satisfying the boundary condition, the step can be completed as above, giving values of s_1, s_2, and s_3 at the end of the step. This step is acceptable if these values are reasonably consistent with the extrapolated values.

If the calculation is started from a stagnation point on a wing, the values for starting the method may be obtained from the similar solution $p = 1$, Section 6.

The size of a cross-flow step will in general be the same as that used in the chordwise calculation. Occasionally, however, it is possible to reduce the number of steps required in the cross flow from that needed for the chordwise. The step size for both calculations depends on the rate of change of the velocity and suction distributions. Smaller steps are needed near stagnation and after a discontinuity in either of these distributions. In the calculation found in Section 5, the smallest step taken was about 0·02 per cent of the chord, and the largest about 10 per cent.

3. *Basic Profiles.* In the previous Section, N has been defined as a linear function of two profiles $f(\eta)$ and $g(\eta)$ where $0 \leqslant \eta \leqslant 1$. Clearly the generality of the method depends on the extent to which N profiles arising in practice can be represented by the f and g profiles chosen. In Fig. 1, three profiles are shown, each scaled such that their maximum value $N_{max} = 1$ and that they reach $1/50\ N_{max}$ (i.e., $N = 0{\cdot}02$) at $\eta = 1$. These profiles have been found to cover the range of shapes of one-sided profiles encountered in a number of exact solutions.

Profile $A(\eta)$ is obtained by suitably scaling the difference of two asymptotic suction T profiles of different thicknesses. In regions of high suction in the adverse pressure-gradient region it has been found that this shape of profile tends to occur frequently. In particular the shape is very much like that of the similar solution suction profiles for $p = -1$.

Profile $S(\eta)$ is the stagnation profile without suction (similar solution $p = 1$), again suitably scaled. It is the dominant shape contributing to the N profile in favourable pressure-gradient regions, even where suction is applied.

Profile $B(\eta)$ is obtained from the difference of two Blasius T profiles of different thicknesses scaled as above. It is likely that this shape occurs as the N profile on an infinite wing for the Howarth flow ($\bar{U} = \bar{U}_0 + \bar{U}_1 X$) in the region where conditions are changing from those of a flat-plate solution $N = 0$.

Since two profiles only may be chosen, it was decided to take $f(\eta) \equiv S(\eta)$ and $g(\eta) \equiv A(\eta) - B(\eta)$, in order to obtain a reasonable coverage of the region. The values of N for these profiles, at intervals of $0{\cdot}05$ in η may be found in Table 1. Note that the $g(\eta)$ profile is of the cross over type.

The expressions found in Section 2.4 may now, therefore, be written:

$$\left.\begin{aligned} a &= -r_1\alpha_1 + r_2\alpha_2 \\ b &= -r_1\beta_1 + r_2\beta_2 \\ s_3 &= \frac{1}{\sigma}(0{\cdot}86523a + 1{\cdot}4849b) \\ s_4 &= \frac{1}{\sigma^2}(0{\cdot}4104a + 2{\cdot}538b) \\ s_1 &= \sigma(4{\cdot}7197a - 1{\cdot}1601b) - r_1 \\ s_2 &= -r_1 d_1 + r_2 d_2 . \end{aligned}\right\} \qquad (17)$$

The coefficients α_1, α_2, β_1, β_2, d_1 and d_2 may be found in Table 2 as functions of l and m for values of $\sigma = 0{\cdot}7$, $0{\cdot}9$, $1{\cdot}0$, $1{\cdot}1$, $1{\cdot}2$ and $1{\cdot}4$.

These tables were computed from similar chordwise profiles obtained from the Falkner-Skan solution (Ref. 3), and a number of T profiles selected from those computed in a recalculation of Head's charts undertaken by A. W. Lindfield of Handley Page Research Department. No tables have been calculated for the separation region, where $l < 0{\cdot}2$, since this region is not required for present purposes.

4. *The Stability of the Three-Dimensional Flow.* Professor Owen first suggested the Reynold's number $\chi = \frac{|n_{max}|}{\nu} z_\Delta$ based on the maximum cross flow $|n_{max}|$, and z_Δ, at which $|n| = 1/10\,|n_{max}|$ as being a suitable criterion for the stability of the cross flow. As long as χ does not exceed its critical value, χ_{crit}, the flow will remain stable.

W. Byron Brown and P. Sayre (Ref. 4) have solved the Orr-Sommerfeld stability equation exactly, for a number of secondary flow profiles in the regions of favourable and adverse pressure gradients with and without suction. They have shown that the critical value of χ, above which disturbances are amplified, depends to a considerable degree on the shape of the profile. They have adopted the value $\left|\partial^2(n/n_{\max})/\partial z/z_\Delta)_{z=0}\right|$ as a shape parameter.

N. Gregory found that if χ_{crit} was plotted against this second derivative, a roughly linear relationship was possible. Thus the value of χ_{crit} may be determined from

$$\chi_{\text{crit}} = 70{\cdot}5 + 0{\cdot}625 \left|\partial^2(n/n_{\max})/\partial z/z_\Delta)_{z=0}\right| .$$

In the notation used previously

$$\frac{\chi}{\chi_{\text{crit}}} = \frac{|N_{\max}|\, 10\sigma\Delta\sqrt{t^*k}}{70{\cdot}5 + 0{\cdot}625\left|\dfrac{(10\sigma\Delta)^2 s_4}{N_{\max}}\right|}, \tag{18}$$

where

$$k = \frac{\bar{U}\bar{V}}{\sqrt{(\bar{U}^2+\bar{V}^2)}}\sqrt{R_c}$$

and Δ is the value of η at which $|N| = \frac{1}{10}|N_{\max}|$.

In Figs. (ii), (iii) and (iv), N profiles of the one-sided and the cross-over type are shown, with the values of $N_{\max}$ and Δ which can be taken.

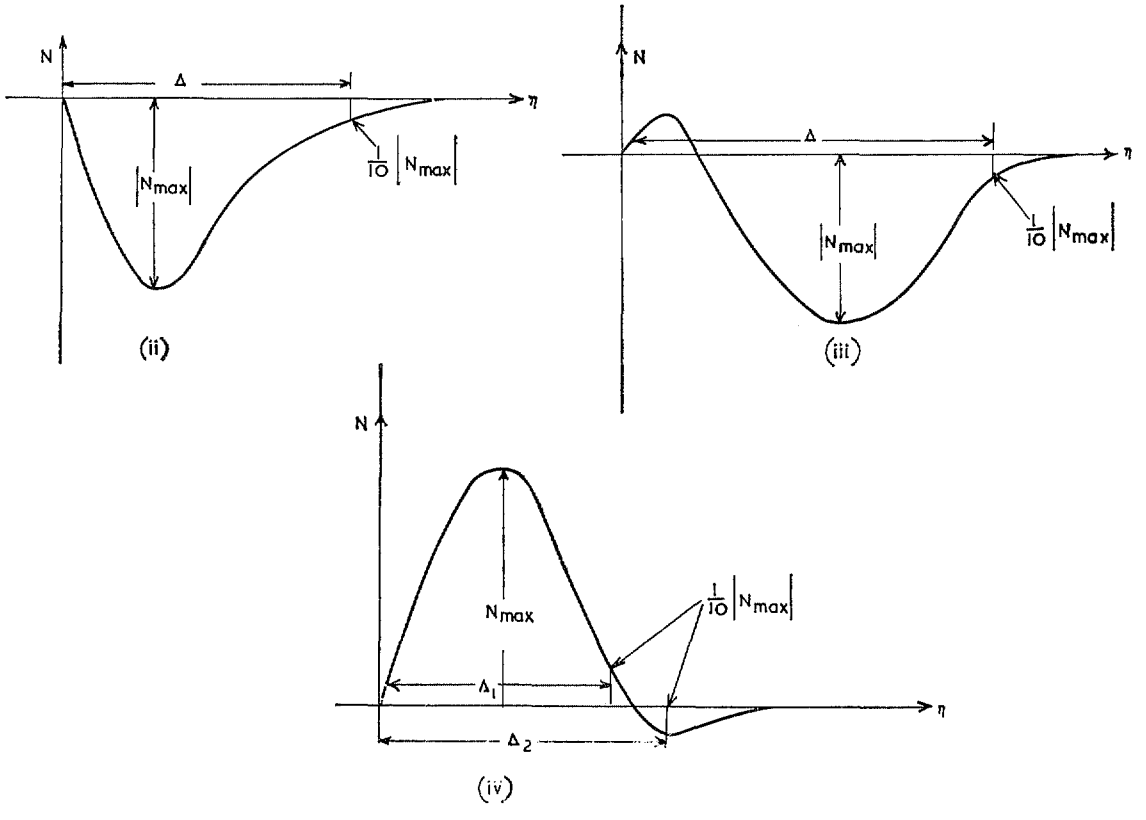

From Fig. (iv), two apparently equally acceptable values of Δ can be taken, giving two distinct values of χ/χ_{crit}. The difference between these values is rarely more than 10 per cent of χ/χ_{crit}.

From Figs. 25 and 26 $N_{\max}$ and Δ can be found, given the values of a and b.

5. *The Method Applied to a Wing.* The object of this calculation was to obtain suction distributions which would ensure stability on the upper and lower surfaces of a wing. The criterion taken was that χ/χ_{crit} should be kept as near to 1·0 as possible, and should not normally be allowed to exceed 1·2, except near the trailing edge. This was a lifting case, where $C_L = 0{\cdot}3$ and the flight Reynolds number was 13×10^6.

For this calculation the boundary-layer Equations (6), (7), (8), (12), (13) and (14) were used in a slightly different form. A variable ϕ was used in place of X. Some three-dimensional effects were included in the equations, not, however, causing any added difficulties in their solution. The wing was treated as a developable surface, the generators of which met at a point. ϕ was the angle made by a generator with the leading edge. Assuming that $\bar{U}$, $\bar{V}$ (velocity components in the ϕ and $-r$ directions), t^* and other non-dimensional quantities are constant along a generator, the equations in their revised form become:

$$\frac{dt^*}{d\phi} = \frac{2}{\bar{U}}\left\{l - \lambda - \left(\frac{d\bar{U}}{d\phi} - \bar{V}\right) t^*(H+2) - \frac{\bar{V}t^*}{2}(1+3s_1-2r_1)\right\} \tag{19}$$

$$\frac{dH_c}{d\phi} = \frac{1}{\bar{U}t^*}\left\{2D^* - \lambda - H_c\left[\frac{\bar{U}}{2}\frac{dt^*}{d\phi} + 3\left(\frac{d\bar{U}}{d\phi} - \bar{V}\right) t^* - \frac{\bar{V}t^*}{2}\right] + \right.$$

$$\left. + \frac{\bar{V}t^*}{2}(7r_2+3s_1-4r_1)\right\} \tag{20}$$

$$\frac{dr_1}{d\phi} = -\frac{1}{\bar{U}t^*}\left\{\left[\frac{\bar{U}}{2}\frac{dt^*}{d\phi} + \left(\frac{d\bar{U}}{d\phi} - \frac{\bar{V}}{2} + \frac{\bar{U}}{\bar{V}}\frac{d\bar{V}}{d\phi}\right) t^*\right] r_1 + \right.$$

$$\left. + \left(\frac{d\bar{U}}{d\phi} - \bar{V} - \frac{\bar{U}^2}{\bar{V}} - \frac{\bar{U}}{\bar{V}}\frac{d\bar{V}}{d\phi}\right) t^*(1+H) + s_3 - \frac{3\bar{V}t^*}{2}\int_0^\infty N^2 dZ\right\} \tag{21}$$

$$\frac{dr_2}{d\phi} = -\frac{1}{\bar{U}t^*}\left\{\left[\frac{\bar{U}}{2}\frac{dt^*}{d\phi} + 2\left(\frac{d\bar{U}}{d\phi} - \frac{3\bar{V}}{2} + \frac{\bar{U}}{\bar{V}}\frac{d\bar{V}}{d\phi}\right) t^*\right] r_2 + \left(\frac{d\bar{U}}{d\phi} - \bar{V}\right) t^* s_1 + \right.$$

$$+ s_3 - 2s_2 + \left(\frac{d\bar{U}}{d\phi} - \bar{V} - \frac{\bar{U}^2}{\bar{V}} - \frac{\bar{U}}{\bar{V}}\frac{d\bar{V}}{d\phi}\right) t^*(1+H-H_c) - \frac{3\bar{V}t^*}{2}\int_0^\infty N^2 dZ +$$

$$\left. + \frac{5\bar{V}t^*}{2}\int_0^\infty N^2 T dZ\right\}, \tag{22}$$

the boundary conditions being

$$m + \lambda l + \left(\frac{d\bar{U}}{d\phi} - \bar{V}\right) t^* = 0 \tag{23}$$

$$s_4 - \lambda s_3 + \left(\frac{d\bar{U}}{d\phi} - \bar{V} - \frac{\bar{U}^2}{\bar{V}} - \frac{\bar{U}}{\bar{V}}\frac{d\bar{V}}{d\phi}\right) t^* = 0. \tag{24}$$

$\bar{V}$ is, of course, for this case no longer a constant. Terms involving cross-flow quantities occur in (19) and (20) and terms involving $\int_0^\infty N^2 dZ$ and $\int_0^\infty N^2 T dZ$ occur in (21) and (22).

In the calculation described here, the extra terms in r_1, r_2 and S_1 of Equations (19) and (20) were not included in the step-by-step computation but a check on their magnitude was made. It was found that this was never sufficiently large to influence the calculation to any significant extent. An approximate idea of the value of the extra terms in (21) and (22) was also obtained and in this calculation, they too were found to be small. If the value of these terms should be needed exactly, a means of determining them will be found in Ref. 9. In the same paper, an account of the derivation of these equations in ϕ is given.

5.1. *The Upper Surface.* In Fig. 2, the velocity distribution for the upper surface is shown plotted against ϕ. This distribution and that for the lower surface were calculated for a tapered wing using Miss Weber's method and including local generator sweep. Pressure was assumed constant along a generator.

In Fig. 3 the suction distribution calculated to stabilise the flow is given, and in Fig. 4, χ/χ_{crit} appropriate to this is shown. Suction was not applied from the leading edge until χ/χ_{crit} approached 1, having started from zero at stagnation ($\phi = -0{\cdot}00035$). Suction was then applied discontinuously to keep χ/χ_{crit} in the region of 1. The suction then fell steadily until $\phi = 0{\cdot}025$ was reached, and it would have been possible to decrease suction still more, since the three-dimensional flow was becoming increasingly stable. However, to avoid the boundary-layer thickness (depending on t^*) becoming too large, and so bringing the two-dimensional stability into doubt, the suction was increased from $\phi = 0{\cdot}025$ onwards. The χ/χ_{crit} continued to fall, reaching a minimum at $\phi = 0{\cdot}054$, and the values of $|N_{\max}|$ previously taken from the negative part of N profile, were subsequently taken from the positive part (*see* Figs. (iii) and (iv)). χ/χ_{crit} then increased rapidly but the flow was kept stable by the increase in suction. At $\phi = 0{\cdot}08$ the situation depicted in Fig. (iv) was reached, necessitating a change over in the definition of Δ and causing an abrupt drop in the value of χ/χ_{crit}. Since some doubt must be attached to the stability criterion for cross-over profiles it would seem that keeping the value of the suction quantity up in this region is well justified. The boundary condition for the cross flow was no longer satisfied from $\phi = 0{\cdot}12$ onwards. An indication of how to deal with this situation is given in Section 8. For $\phi > 0{\cdot}14$, the accuracy of the chordwise charts could not be relied upon, so some doubt attaches to the results.

5.2. *The Lower Surface.* The velocity distribution is given in Fig. 5, and in Fig. 6 two suction distributions I and II are shown, differing from $\phi = 0{\cdot}033$ onwards but amounting to the same overall suction quantity. The corresponding χ/χ_{crit} curves are shown in Fig. 7. Examination of Figs. 6 and 7 discloses that comparatively little change occurs in the χ/χ_{crit} distribution for the two suction cases. It seems, therefore, that any extra suction applied early on, as in case II, is not wasted but plays its part in stabilizing the later flow.

For the lower surface two comparisons have been made. In the favourable pressure-gradient region, the method was thought to be reasonably accurate for two reasons. Firstly, the profile adhered very closely to the shape of the stagnation profile (*i.e.*, $b \ll a$) and secondly, the values of l and m obtained in the chordwise calculation were always on the Falkner-Skan solution line (*cf.* Section 3).

Comparison from $\phi = 0{\cdot}00035$ *to* $\phi = 0{\cdot}033$. To demonstrate a quick calculation taking only a few hours it was assumed that σ, the thickness parameter, was fixed at a value of $1{\cdot}2$†. Considering,

† Another approximation would be to take $b = 0$ but such a solution would differ little from the solution already obtained. In this solution the average value of σ was $1{\cdot}05$.

therefore, only the boundary condition (14) and the r_1' Equation (12), which were reduced to the one equation $r_1' = Pr_1 + Q$ where P and Q are functions only of the chordwise flow, r_1 was obtained and compared with that of the first solution in Fig. 12. The profiles obtained by the two methods are compared in Figs. 8 and 9. The χ/χ_{crit} obtained by the simplified method is shown in Fig. 7. This method is too approximate to be used accurately in the adverse pressure-gradient region.

Comparison $\phi = 0{\cdot}033$ *to* $\phi = 0{\cdot}14$. From $\phi = 0{\cdot}033$ onwards, Case II, with the smooth suction distribution, was repeated using an adapted form of the differential method (Ref. 1). A description of this process will be found in Appendix III. Comparisons of the profiles are shown in Figs. 10 and 11, and of the χ/χ_{crit} in Fig. 7. The values calculated for r_1 and r_2 are shown in Figs. 12 and 13. In the integral method, the cross-flow boundary condition was again not satisfied for $\phi \geqslant 0{\cdot}12$, but the profiles in comparison with the differential method show reasonable agreement as least as far as $\phi = 0{\cdot}14$. The comparison of χ/χ_{crit} indicates that no change to the suction would be required.

As an indication of the time taken for a typical calculation using the integral method the upper-surface calculation above took two people one week. The chordwise steps taken totalled about forty, the cross flow about thirty. Naturally a lot depends on the initial conditions and the velocity distribution. It would take much less time if a suction distribution was initially fixed instead of being calculated at each step to ensure stability.

6. *Similar Solutions.* A number of exact solutions for the infinite swept wing exist where the velocity distribution is in the form $U = U_0 X^n$. For this velocity distribution the boundary-layer equations can be transformed in such a way that the velocity profiles are seen to be of similar shape. The integral method described in this paper has been compared with a few representative solutions.

In the chordwise flow, since the T profile has the same shape everywhere l and m are constant. Defining a non-dimensional momentum thickness for the assumption that $p \neq -1$

$$\Theta = \frac{\theta}{x}\left(\frac{Ux}{\nu}\right)^{1/2}\left(\frac{p+1}{2}\right)^{1/2} = X^{(p-1)/2}\sqrt{\left(\frac{p+1}{2}\,t^*\right)}$$

and a suction quantity

$$K = -W_0\, X^{-(p-1)/2}\sqrt{\left(\frac{2}{p+1}\right)},$$

then chordwise Equations (6) and (7) become, noting that $H_c' = 0$

$$\Theta^2 = \frac{p+1}{1-p}\,[l - \Lambda(H+2) - \lambda] \tag{25}$$

$$2D^* - H_c[l - (H-1)\Lambda - \lambda] - \lambda = 0, \tag{26}$$

the boundary condition (8) remaining the same, but with $\Lambda = 2p\,\Theta^2/(p+1)$, $\lambda = K\Theta$. To obtain the chordwise solution given K and p, these equations can be solved to yield Θ, l and m. A fuller description is given in Ref. 2.

In the cross flow, the N profile also has the same shape everywhere and hence r_1 and r_2 are constants. Since r_1' and r_2' are zero, Equations (12) and (13) become:

$$-r_1\Theta^2 - (1+H)\Lambda - s_3 = 0 \tag{27}$$

$$-r_2(\Theta^2+\Lambda) - (1+H-H_c)\Lambda + 2s_2 - s_3 - \Lambda s_1 = 0, \tag{28}$$

the boundary condition (14) being unchanged here also.

These equations can be solved using the relationships in Section 3, expressing each equation in terms of a, b and σ.

Using Ref. 5 and Ref. 6 for some of the exact solutions required, comparisons were made which appear in Figs. 14 to 16. In Fig. 14 is the stagnation solution $p = 1$. Since this is one of the basic N profiles used in the cross-flow method and the stagnation T profile is one of the Falkner-Skan range of solutions which were used in computing the charts, any discrepancy between the exact solution and the calculated one would appear to arise from the chordwise solution. Indeed in most of the calculations made for similar solutions, certain inaccuracies were encountered due to a greater dependence of the cross flow on the approximate chordwise method, especially for the higher suction cases. In Fig. 15 is shown the comparison between the exact and approximate solutions for the $p = -1/11$, $K = 0{\cdot}4$ profile. For the case $p = -1/3$, two values of the suction quantity have been considered. Both results are given in Fig. 16, and that for $K = 1{\cdot}554$ is adequate. However, for $K = 2{\cdot}543$, the discrepancy between the two solutions obtained and the exact solution was directly traceable to the chordwise inaccuracies. In the two solutions referred to, one used the method as indicated in Section 3, in which the boundary condition could not be satisfied. The other was a solution obtained using the adapted form of the method as indicated in the next section, and the boundary condition was satisfied.

7. *Comparison of Method with an Exact Solution.* In Fig. 17 there appears a velocity distribution and a suction distribution used in a calculation done in America by W. Pfenninger (Ref. 8). A digital computer was used. The flight Reynolds number was 10×10^6. In his report he publishes also the N profiles obtained for this and three other suction cases used with the same velocity distribution. Hence comparisons of the present method with his results can be made. Two points should be noted. Firstly at $63{\cdot}11$ per cent chord there is a discontinuity in the slope of the velocity distribution, and a discontinuous start in suction. Secondly, in this case (referred to by Pfenninger as A_1) there is insufficient suction for stabilising the flow. In his other cases, in none of which the profile shapes seem so radically different as to be impossible to obtain by this method, he claims stability for the region between $63{\cdot}11$ per cent and 100 per cent, but in no case has any suction been applied before $63{\cdot}11$ per cent. It might be noted that the Pfenninger calculation used here was also used for comparison in Ref. 1.

In Figs. 18 and 19 comparisons of N obtained up to $63{\cdot}11$ per cent are shown. In this region the profile was very similar in shape to a stagnation one and the calculation of l and m gave a line coincident with the Falkner-Skan similar solution line in the l, m plane. In fact a calculation has been made using the stagnation type of profile only, yielding very good comparisons, but clearly this approach lacks generality and a calculation of such a type would be less satisfactory where suction was applied.

From $63{\cdot}11$ per cent several calculations have been made. In Figs. 20 and 21, it may be seen that the original calculation, carrying straight through the discontinuity ignoring any possible difficulties, yields less satisfactory results for the 64 per cent and 65 per cent cross-over profiles but that by the time the 70 per cent and 80 per cent profiles are reached, reasonable agreement is achieved. From 80 per cent, unfortunately, another difficulty is encountered. As referred to in Section 8 the boundary condition (Equation 14) is frequently not satisfied for a profile where large suction is being applied, and this is what happens here. The method referred to there is applied and two results for the 80 per cent and 90 per cent profiles are shown. As might be expected the

difference in the results for the 80 per cent profile is not significant, but for the 90 per cent profile a considerably better shape is obtained by using the stagnation profile with the asymptotic one, the boundary condition then being satisfied. In Figs. 22 and 23 the two calculations of r_1 and r_2 are shown with the exact results obtained from Pfenninger's calculations.

Returning to Fig. 20 another comparison appears. From 63·11 per cent, it was considered that a reasonable method of taking into account the discontinuity was to fix or 'freeze' the 63·11 per cent profile, and allow another profile to grow from zero (*cf.* 9.1). This additional profile was taken to be directly of the asymptotic type, and it may be seen that much more satisfactory results were obtained this way.

The r_1 was taken to be the same as that obtained from the original calculation. Clearly such a method could be extended throughout the whole of the region where cross-over profiles occur.

8. *Alternative Basic Profiles.* Referring back to Section 3 where two basic profiles $f(\eta) \equiv S(\eta)$ and $g(\eta) \equiv A(\eta) - B(\eta)$ are given, it is possible that it may be better in certain circumstances to choose a different representation for N. An example of this is where the boundary condition is no longer satisfied.

$$\begin{aligned} &\text{Let } N = af(\eta) + bg(\eta) + ch(\eta), \qquad 0 \leqslant \eta \leqslant 1, \qquad \eta = Z/10\sigma \\ &\qquad N = 0, \qquad\qquad\qquad\qquad \eta > 1, \end{aligned} \tag{29}$$

where the profile shape $h(\eta) \equiv A(\eta)$ is included directly.

If

$$\left.\begin{aligned} \int_0^\infty h(\eta)\,T\,dZ &= \gamma_1 \\ \int_0^\infty h(\eta)\,T(1-T)\,dZ &= \gamma_2 \\ \int_0^\infty \frac{dh}{dZ}\frac{dT}{dZ}\,dZ &= d_3, \end{aligned}\right\} \tag{30}$$

where γ_1, γ_2 and d_3 are known functions of σ, l and m, and

$$\begin{aligned} \frac{1}{10}\left(\frac{dh}{d\eta}\right)_{\eta=0} &= 1{\cdot}857 \\ \frac{1}{100}\left(\frac{d^2h}{d\eta^2}\right)_{\eta=0} &= 2{\cdot}538 \\ 10\int_0^1 h(\eta)\,d\eta &= 3{\cdot}96363, \end{aligned}$$

then since N is assumed linear in terms of parameters a, b and c, it may be seen that instead of Equations (17), the system below is obtained.

$$\left.\begin{aligned} a &= -(r_1 - c\gamma_1)\alpha_1 + (r_2 - c\gamma_2)\alpha_2 \\ b &= -(r_1 - c\gamma_1)\beta_1 + (r_2 - c\gamma_2)\beta_2 \\ s_1 &= \sigma[4{\cdot}7197a - 1{\cdot}1601b + 3{\cdot}9636c] - (r_1 - c\gamma_1) \\ s_2 &= -(r_1 - c\gamma_1)d_1 + (r_2 - c\gamma_2)d_2 + cd_3 \\ s_3 &= \frac{1}{\sigma}(0{\cdot}86523a + 1{\cdot}4849b + 1{\cdot}8570c) \\ s_4 &= \frac{1}{\sigma^2}(0{\cdot}4104a + 2{\cdot}5380b + 2{\cdot}5380c). \end{aligned}\right\} \tag{31}$$

The definition of N given in (23) involves four parameters, of which only three can be found by the exact method, unless an extra integral equation is introduced. Such an equation could be derived from Equation (11) by taking $j(T, N) = T^2$. Although such a method might be expected to give greater accuracy due to the greater diversity of shapes which could be predicted for the N profile, it would take half as long again in use, once a new system of charts had been obtained. In practice, to reduce the number of parameters some assumption must be made. For example, σ could be fixed, yielding a simple set of equations linear in the unknown parameters a, b and c. This system would have the advantages of incorporating all three basic profile shapes given in Fig. (1) and would presumably always satisfy the boundary condition.

The above Equations (31) have been used with the assumption that $b = 0$, that is the profiles used were the stagnation (S) and asymptotic (A) only. Such a system has been used to obviate difficulties met previously in satisfying both the boundary condition and the r_1 and r_2 equations (as for example where high suction is needed in the adverse pressure-gradient region, where the profile tends to be of the asymptotic type). The values of the profile $h(\eta)$ for intervals of $0{\cdot}05$ in (η) can be found in Table 1.

An alternative system for use when the boundary conditions fail, particularly for large values of l, has also been evolved. This system uses the stagnation $S(\eta)$ profile, and a cross-over profile obtained as the difference of the asymptotic and the stagnation profiles $A(\eta) - S(\eta)$. For this system the expressions for use in the method become:

$$\left.\begin{aligned}
r_1 &= a\int_0^1 f\,T d\eta + \bar{c}\int_0^1 (h-f)\,T d\eta \\
r_2 &= a\int_0^1 f\,T(1-T) d\eta + \bar{c}\int_0^1 (h-f)\,T(1-T) d\eta \\
a &= -r_1\delta_1 + r_2\delta_2 \\
\bar{c} &= -r_1\epsilon_1 + r_2\epsilon_2 \\
s_1 &= \sigma[4{\cdot}7197a - 0{\cdot}7561\bar{c}] - r_1 \\
s_2 &= ad_4 + \bar{c}d_5 \\
s_3 &= \frac{1}{\sigma}[0{\cdot}8652a + 0{\cdot}9918\bar{c}] \\
s_4 &= \frac{1}{\sigma^2}[0{\cdot}4104a + 2{\cdot}1276\bar{c}],
\end{aligned}\right\} \qquad (32)$$

where δ_1, δ_2, ϵ_1, ϵ_2, d_4 and d_5 may be found from Table 2 and $h(\eta) - f(\eta)$ may be obtained from Table 1. The expressions are given for the III and IV lines, *see* Fig. 24. The IV line is defined by:

$$\begin{aligned}
l &= 0{\cdot}5243, \qquad & m &= -0{\cdot}399 \\
l &= 0{\cdot}759, & m &= -0{\cdot}978 \\
l &= 1{\cdot}021, & m &= -1{\cdot}523.
\end{aligned}$$

9. *Concluding Remarks.* 9.1. At a discontinuity in suction or in the velocity gradient r_1 and r_2 may be assumed to be continuous. All other quantities should be obtained immediately after the discontinuity, using these values of r_1 and r_2 and the boundary condition in the usual way. If the discontinuity is large, it may be found that the method gives the integral quantities satisfactorily

but that a small distance along the boundary layer is needed before the profile used in the method gives a reasonable fit. An alternative method which is likely to give better results is to fix or 'freeze' the profile before the discontinuity and allow an additional profile to be determined to take into account conditions after the discontinuity.

9.2. A simplification which might be made if a quicker determination were needed would be to take values in the favourable pressure gradient along the I (Falkner-Skan) line only, of Fig. 24. The method could also be simplified in this region by taking the stagnation profile only and neglecting the r_2 equation.

9.3. Some clarification of the stability criterion for cross-over profiles (Section 4) would appear to be desirable, since the definition of χ for these profiles is not particularly satisfactory. Perhaps it would be possible to define some alternative measure based on integral quantities which might then be fitted more directly into the method.

It is believed that the stability criterion used here (*i.e.*, $\chi/\chi_{\text{crit}} = 1$) is pessimistic. Doubt must remain until more experimental work on the stability of the three-dimensional boundary layer is performed.

Acknowledgements. This work was carried out under the direction of Dr. G. V. Lachmann, Director of Research, Handley Page Ltd. The authors would like to express their thanks to Mr. J. B. Edwards and Mr. A. W. Lindfield of the Handley Page Research Department for their valuable interest and advice.

NOTATION

x, y, z		Co-ordinates in the chordwise, spanwise and vertical directions
u, v, w		Components of velocity in the x, y, z directions
U_∞		Flight velocity
U_0		Chordwise component of U_∞
V_0		Spanwise component of U_∞
U		Local chordwise outer-flow velocity
$\bar{U}$	$=$	U/U_0
$\bar{V}$	$=$	V_0/U_0
ν		Coefficient of kinematic viscosity
c_0		Chord perpendicular to the leading edge measured in the chordwise direction
$\bar{c}_0$		Chord in flight direction
R_c		Chordwise Reynolds number $U_0 c_0/\nu$
$R_{\bar{c}}$		Flight Reynolds number $(U\infty \bar{c}_0)/\nu$
k	$=$	$\dfrac{\bar{U}\bar{V}}{\sqrt{(\bar{U}^2+\bar{V}^2)}}\sqrt{R_c}$
n		Cross-flow velocity $= \dfrac{kU_0}{\sqrt{R_c}}\left(\dfrac{v}{V_0}-\dfrac{u}{U}\right)$
T	$=$	u/U
S	$=$	v/V_0
N	$=$	$S-T$
θ	$=$	$\int_0^\infty T(1-T)dz$
t^*	$=$	$(\theta/c_0)^2 R_c$
X	$=$	x/c_0
Z	$=$	$z/c_0 \dfrac{\sqrt{R_c}}{\sqrt{t^*}}$
w_0		Velocity w at boundary $z = 0$
W_0	$=$	$\dfrac{w_0}{U_0}\sqrt{R_c}$
λ	$=$	$-W_0\sqrt{t^*}$
Λ	$=$	$\bar{U}' t^*$
l	$=$	$\left(\dfrac{\partial T}{\partial \bar{Z}}\right)_{Z=0}$
m	$=$	$\left(\dfrac{\partial^2 T}{\partial \bar{Z}^2}\right)_{Z=0}$

NOTATION—*continued*

$H = \int_0^\infty (1-T)dZ$ (dependent on displacement thickness)

$H_e = \int_0^\infty T(1-T^2)dZ$ (dependent on energy thickness) (*see* Ref. 7)

$D^* = \int_0^\infty \left(\frac{\partial T}{\partial Z}\right)^2 dZ$ (dissipation integral)

$r_1 = \int_0^\infty NTdZ$

$r_2 = \int_0^\infty NT(1-T)dZ$

$s_1 = \int_0^\infty N(1-T)dZ$

$s_2 = \int_0^\infty \frac{\partial N}{\partial Z} \times \frac{\partial T}{\partial Z} dZ$

$s_3 = \left(\frac{\partial N}{\partial Z}\right)_{Z=0}$

$s_4 = -\left(\frac{\partial^2 N}{\partial Z^2}\right)_{Z=0}$

a, b, c, σ Parameters used in the definition of N.

$\eta = Z/10\sigma$

$\alpha_1, \alpha_2, \beta_1, \beta_2, \gamma_1, \gamma_2, d_1, d_2, d_3$ Functions of l, m and σ

$|n_{\max}|$ Maximum value of n

$|N_{\max}|$ Maximum value of N

z_Δ Value of z at which $|n| = \frac{1}{10}|n_{\max}|$

Δ Value of η at which $|N| = \frac{1}{10}|N_{\max}|$

$\chi = \frac{|n_{\max}|z_\Delta}{\nu} = |N_{\max}|(10\sigma\Delta)k\sqrt{t^*}$

χ_{crit} Critical value of χ

p Similar solution parameter derived from $U = U_0 X^p$

$\Theta = X^{(p-1)/2}\left(\frac{p+1}{2}\right)^{1/2}\sqrt{t^*}$

$K = -W_0\sqrt{\left(\frac{2}{p+1}\right)}X^{-(p-1)/2}$

Dashes denote total differentiation with respect to X

REFERENCES

No.	*Author*	*Title, etc.*
1	A. W. Lindfield and H. G. Pinsent ..	An approximate method for calculating the laminar boundary layer on an infinite swept wing with arbitrary velocity and suction distributions. A.R.C. C.P. 516. July, 1957.
2	M. R. Head	An approximate method of calculating the laminar boundary layer in two-dimensional incompressible flow. A.R.C. R. & M. 3123. March, 1957.
3	A. M. O. Smith	Improved solutions of the Falkner and Skan boundary layer equation. I.A.S. Fairchild Fund Paper. FF.10. 1954.
4	W. Byron Brown and P. Sayre ..	An exact solution of the Orr-Sommerfeld stability equation for low Reynolds numbers. Northrop Report No. BLC-43.
5	B. Thwaites	The development of the laminar boundary-layers under conditions of continuous suction. Part II. A.R.C. 12,699. November, 1949.
6	K. D. P. Sinha	The laminar boundary layer with distributed suction on an infinite yawed cylinder. A.R.C. C.P. 214. November, 1954.
7	K. Wieghardt	On an energy equation for the calculation of laminar boundary layers. GDC 10/4256 T (R. and T. No. 89). 1946.
8	W. Pfenninger, G. S. Raetz and W. B. Brown.	Note on design problems of swept laminar suction wings. Northrop Aircraft Inc., Report No. NAI 55-549 BLC-79.
9	G. V. Lachmann (*Editor*)	*Boundary Layer and Flow Control—Principles and Applications* (Pergamon Press). Part II, Chap. V—Approximate methods for calculating three-dimensional boundary layer flow on wings.

APPENDIX I

Expressions for use in the Chordwise Method

As an alternative to the charts of Ref. 2 the following expressions may be used.

$$l(1-0{\cdot}44\lambda) = 0{\cdot}342 + 1{\cdot}52(H_c - 1{\cdot}64) + 1{\cdot}667(H_c - 1{\cdot}64)^2 + 0{\cdot}44\Lambda,$$

where

$$H_c \geqslant 1{\cdot}62.$$

$$l(1-0{\cdot}44\lambda) = 0{\cdot}2726 + 1{\cdot}0901(H_c - 1{\cdot}60) + 0{\cdot}44\Lambda \quad \text{where} \quad H_c < 1{\cdot}62.$$

$$H = 2{\cdot}99 - 2{\cdot}23l - 0{\cdot}5l^2 - m, \qquad l \geqslant 0{\cdot}4$$

$$H = 3{\cdot}488 - 4{\cdot}57l + 2{\cdot}28l^2 - m, \qquad l < 0{\cdot}4$$

$$2D^* = 0{\cdot}303 + 1{\cdot}111l^2 + 0{\cdot}3365m, \qquad l \geqslant 0{\cdot}4$$

$$2D^* = 0{\cdot}228 + 0{\cdot}423l + 0{\cdot}524l^2 + 0{\cdot}3365m, \qquad l < 0{\cdot}4.$$

APPENDIX II

In Table 2 the values of constants A, B and C will be found and can be substituted in the expression

$$\delta = A + Bl + Cl^2 \text{ for any chosen value of } \sigma$$

where δ is any one of the quantities α_1, α_2, β_1, β_2, γ_1, γ_2, d_1, d_2 and d_3. These expressions, embodying as much accuracy as the original computed points, may be found more convenient for computation. Numbers I, II and III refer to the three lines used in the l, m plane which are shown in Fig. 24. It has been found that linear interpolation for the value of m required, using this figure, gives sufficiently accurate results in practice, although of course a more accurate method of interpolation can be used if desired. It has also been found that in the favourable pressure-gradient region except after discontinuities, the values of l and m give points very close to line I, the Falkner-Skan similar solution line.

δ_1, δ_2, ϵ_1, ϵ_2, d_4 and d_5 may also be calculated. It should also be noted that interpolation between III of Fig. 24 and IV, given by $l = 0{\cdot}5243$, $m = -0{\cdot}399$; $l = 0{\cdot}759$, $m = -0{\cdot}978$; and $l = 1{\cdot}021$, $m = -1{\cdot}523$, must be done where needed.

APPENDIX III

Differential Method

Returning to Equation (9) of Section 2.3 and putting $W_0 = -\frac{\lambda}{\sqrt{t^*}}$ the equation may be rewritten

$$\bar{U}T\frac{\partial N}{\partial X} = -(1-T^2)\bar{U}' - \frac{\partial N}{\partial Z}\left[\frac{-\lambda}{t^*} - \int_0^z \frac{\partial}{\partial X}(\bar{U}T)dZ - \right.$$
$$\left. - \frac{t^{*\prime}}{2t^*}\int_0^z \bar{U}TdZ\right] + \frac{1}{t^*}\frac{\partial^2 N}{\partial Z^2}$$

where all the coefficients of $\partial N/\partial X$, $\partial N/\partial Z$, $\partial^2 N/\partial Z^2$ can be derived from the chordwise solution. From the remaining charts of Ref. 2 the values of T for each value of Z can be obtained. Sufficient values of Z should be chosen to give adequate coverage of all the quantities involved. Ten values of Z were used in the following calculation. It is possible to perform a step-by-step method, starting from an N profile and determining its first and second derivatives† with respect to Z, and by substituting these in the above equation finding $\partial N/\partial X$ and hence a value of N at the next step.

For comparison purposes in calculation II of the lower surface of Section 5 the differential method was started at a value $\phi = 0{\cdot}033$. Values of N given by the integral method at this point were used, and once approximate values of the derivatives had been obtained, the equation was used to achieve consistency. This starting point was chosen for two reasons. Firstly it was considered that the integral method was reasonably accurate over the region near to stagnation, and secondly the differential method has not as yet been used where the values of $\bar{U}$ are small since difficulties might be anticipated. The starting values at $0{\cdot}033$ are shown in Fig. 10, and comparisons as far as $\phi = 0{\cdot}14$ for this calculation are shown in Figs. 10 and 11. In Figs. 12 and 13 the values of r_1 and r_2 calculated using this method are shown. As a check on how important the starting values were in the calculation by the differential method, another calculation was done using starting values from the profile obtained by the integral method at $\phi = 0{\cdot}043$. By the time a few small steps had been taken as far as $\phi = 0{\cdot}051$, the values computed in this calculation by the differential method were practically coincident with those of the previous determination, as indicated in Fig. 10.

It is considered likely that the shapes of the cross-over profiles $\phi = 0{\cdot}051$ and $\phi = 0{\cdot}06$ may be more adequately represented by the differential method but the degree of accuracy of this method is not yet certain.

In addition to any possible difficulties near stagnation, the differential method is not so easily adapted for a calculation where all values from the suction and the chordwise solution are not smooth. Hence it is not very practicable to use it to determine a suction distribution where a step in the cross flow normally follows a single step in the chordwise flow making it difficult to ensure that all values put into the equation will be smooth. It also takes a longer time for the computation which makes it less useful where a large number of such calculations must be done.

Two differences between the differential method as used here and in Ref. 1 should be noted. Firstly, it was used directly rather than in the form of a difference differential equation and secondly, the variable Z was used instead of $(z/c)\sqrt{R}$. The advantage of this was that Z changed very little in the course of the calculation and did not increase with the boundary-layer thickness.

† This can be done by a graphical or a numerical procedure, using the boundary condition to ensure accurate values at the wall $Z = 0$, this process being sufficiently accurate to obtain consistent results for a small step.

TABLE 1

Values of $f(\eta)$, $g(\eta)$, $h(\eta)$

η	$f(\eta)$	$g(\eta)$	$h(\eta)$
0	0	0	0
0·05	0·377	0·454	0·657
0·10	0·651	0·556	0·933
0·15	0·853	0·452	1·0
0·20	0·963	0·240	0·942
0·25	1·0	0	0·840
0·30	0·969	−0·225	0·716
0·35	0·8925	−0·3985	0·600
0·40	0·794	−0·503	0·490
0·45	0·686	−0·559	0·397
0·50	0·570	−0·555	0·306
0·55	0·453	−0·500	0·240
0·60	0·354	−0·425	0·185
0·65	0·264	−0·331	0·140
0·70	0·191	−0·241	0·110
0·75	0·138	−0·163	0·083
0·80	0·096	−0·100	0·063
0·85	0·065	−0·058	0·048
0·90	0·041	−0·029	0·036
0·95	0·028	−0·009	0·025
1·00	0·020	0	0·020

TABLE 2

		I			II			III		
		A	*B*	*C*	*A*	*B*	*C*	*A*	*B*	*C*
$\sigma = 0{\cdot}7$	α_1	1·42863	−4·65397	4·19504	1·52186	−4·68536	4·01140	1·23621	−3·19058	2·37837
	α_2	5·15201	−11·91875	12·43286	5·06117	−10·31592	9·25198	4·51023	−7·04055	5·41522
	β_1	3·70376	−8·42811	7·60175	3·59787	−7·23289	5·69458	3·89160	−8·33467	7·10079
	β_2	7·77082	−13·65939	16·16487	7·44219	−10·85574	10·92834	7·19487	−8·78942	7·98335
	d_1	−0·37949	1·75110	−1·59827	−0·38116	1·72516	−1·44512	−0·15829	0·57488	0·06584
	d_2	−1·02680	4·91439	−2·23859	−1·06075	4·92194	−2·10106	−0·75522	3·18549	0·20549
	γ_1	0·61158	2·74914	−1·64083	0·61254	2·42599	−1·07072	0·77602	1·67862	−0·54185
	γ_2	0·40991	0·64209	−0·77620	0·36691	0·82816	−0·96295	0·53064	−0·00951	0·08411
	d_3	−0·14444	0·86762	0·17488	−0·19778	1·15080	−0·29761	−0·15107	0·88445	−0·02201
$\sigma = 0{\cdot}9$	α_1	0·41226	−1·55801	1·54636	0·34609	−1·08390	0·83058	0·27883	−0·75702	0·51036
	α_2	2·58224	−4·66233	5·16728	2·36554	−3·23970	2·98230	2·44871	−3·42398	2·98675
	β_1	1·42819	−2·44636	2·29383	1·28624	−1·52174	0·99565	1·29993	−1·59768	1·22099
	β_2	3·90344	−4·05920	6·41071	3·45638	−1·72104	3·12033	3·26091	−0·67007	1·36632
	d_1	−0·21263	0·88051	−0·67944	−0·23098	0·92526	−0·67531	−0·15985	0·50183	−0·10883
	d_2	−0·68190	3·25254	−0·85201	−0·74758	3·33501	−0·84996	0·87843	−4·26495	7·22951
	γ_1	1·16928	3·16683	−1·83587	1·14643	2·94491	−1·42305	1·14276	2·90833	−1·67792
	γ_2	0·53313	0·71487	−1·08948	0·54559	0·60931	−0·85528	0·54596	0·51083	−0·57372
	d_3	−0·14943	1·12582	−0·27121	−0·18194	1·23070	−0·43348	−0·20811	1·28637	−0·53483
$\sigma = 1{\cdot}0$	α_1	0·19971	−0·82647	0·76175	0·16239	−0·60702	0·48247	0·13690	−0·47232	0·33573
	α_2	1·99081	−3·07638	3·46732	1·90692	−2·62882	2·82866	1·70370	−1·42842	1·14832
	β_1	0·95659	−1·21161	1·00167	0·88353	−0·78351	0·45830	0·85955	−0·72837	0·51913
	β_2	3·06516	−2·18291	4·38712	2·45512	0·76148	0·46593	2·47284	0·71272	0·15776
	d_1	−0·16563	0·65782	−0·47009	−0·17892	0·68656	−0·46865	−0·16243	0·53185	−0·23345
	d_2	−0·55374	2·64472	−0·28388	−0·56142	2·46420	−0·04505	−0·81844	3·48548	−1·35026
	γ_1	1·48601	3·33245	−1·93699	1·46704	3·18686	−1·73211	1·41910	3·28488	−2·06980
	γ_2	0·58174	0·75135	−1·24068	0·60629	0·59892	−0·94364	0·68595	0·10514	−0·18635
	d_3	−0·13516	1·14040	−0·33290	−0·16945	1·24807	−0·49934	−0·27053	1·62903	−0·93031

TABLE 2—*continued*

		I			II			III		
		A	*B*	*C*	*A*	*B*	*C*	*A*	*B*	*C*
$\sigma = 1{\cdot}1$	α_1	0·07996	−0·44673	0·39672	0·11075	−0·55459	0·48890	0·02953	−0·20371	0·12724
	α_2	1·61879	−2·26248	2·72056	1·49482	−1·44859	1·50879	1·52381	−1·47807	1·32338
	β_1	0·73194	−0·93023	0·90480	0·67095	−0·57660	0·43583	0·61128	−0·33192	0·21641
	β_2	2·69133	−2·19317	5·01926	2·26661	−0·33644	2·42299	1·71609	2·76491	−2·01086
	d_1	−0·12791	0·48132	−0·30062	−0·13979	0·51055	−0·31587	−0·14035	0·45963	−0·22661
	d_2	−0·46333	2·26831	−0·04188	−0·45266	2·01535	0·25233	−0·56909	2·45773	−0·51290
	γ_1	1·19748	2·38051	−0·20611	1·83033	3·11824	−1·51364	1·89282	2·76963	−1·49440
	γ_2	0·70541	0·17402	−0·33824	0·70807	0·24449	−0·50992	0·63922	0·52400	−0·69706
	d_3	−0·10812	1·06076	−0·25381	−0·14370	1·19192	−0·47340	−0·19751	1·35895	−0·67298
$\sigma = 1{\cdot}2$	α_1	0·04301	−0·42262	0·47013	0·06552	−0·47793	0·46347	−0·01276	−0·11778	0·06624
	α_2	1·42251	−2·08322	2·73977	1·34061	−1·45620	1·66701	1·27071	−1·02015	0·94814
	β_1	0·59341	−0·87368	1·07318	0·51714	−0·38280	0·33090	0·46990	−0·18204	0·11982
	β_2	2·45601	−2·32973	5·37251	2·10876	−0·57616	2·66882	1·46296	2·77947	−1·90384
	d_1	−0·09926	0·34658	−0·16728	−0·10998	0·38017	−0·20322	−0·10966	0·34486	−0·15627
	d_2	−0·37401	1·89269	0·24719	−0·39412	1·83351	0·23692	−0·48705	2·21133	−0·48806
	γ_1	2·20642	3·44687	−1·96753	2·24595	2·90930	−1·18299	1·88398	4·38800	−3·07536
	γ_2	0·70044	0·48509	−0·94365	0·73103	0·30807	−0·62640	0·66455	0·55993	−0·77204
	d_3	−0·09984	1·11198	−0·39302	−0·13862	1·25628	−0·61908	−0·13180	1·12063	−0·46097
$\sigma = 1{\cdot}4$	α_1	−0·01757	−0·22341	0·25655	0·03648	−0·44560	0·48218	−0·05548	−0·01787	−0·00577
	α_2	1·12833	−1·57768	2·29293	1·17676	−1·66654	2·01006	1·09020	−1·10779	1·12972
	β_1	0·39287	−0·55838	0·79941	0·39707	−0·50868	0·62123	0·33781	−0·18670	0·17874
	β_2	1·94314	−1·14120	3·58825	2·06135	−1·24206	2·91459	2·01945	−1·23837	2·45530
	d_1	−0·06109	0·17916	−0·01817	−0·07481	0·23688	−0·09496	−0·05692	0·14918	−0·01993
	d_2	−0·22093	1·22846	0·80118	−0·38041	2·03112	−0·42458	−0·24742	1·41074	−0·05529
	γ_1	3·52931	−0·24339	4·19783	2·84263	3·64946	−2·05232	3·03181	2·78696	−1·29364
	γ_2	0·51552	2·18803	−3·92074	0·61685	1·20950	−1·90790	0·89215	−0·18138	−0·04765
	d_3	−0·04579	0·99240	−0·41667	−0·09293	1·15877	−0·60764	−0·04816	0·86199	−0·28224

TABLE 2—*continued*

		III			IV		
		A	*B*	*C*	*A*	*B*	*C*
$\sigma = 0{\cdot}9$	δ_1	0·62817	−1·29865	0·74099	0·21694	−0·04228	−0·04780
	δ_2	2·67318	−1·67175	0·73927	1·57585	1·17644	−0·70754
	ϵ_1	3·28925	−3·00440	1·20527	2·07053	0·08108	−0·25281
	ϵ_2	9·19541	−1·65201	0·28903	9·62400	−3·93164	3·05051
	d_4	−0·15720	1·24740	−0·75054	0·24346	−0·26778	0·31720
	d_5	−0·05565	0·05955	0·19436	−0·10806	0·27288	−0·02192
$\sigma = 1{\cdot}0$	δ_1	0·45524	−1·07463	0·75974	0·15206	−0·11053	0·02346
	δ_2	2·75608	−2·94032	2·22024	2·16361	−0·91191	0·50090
	ϵ_1	2·71395	−3·45711	2·40294	1·53511	0·15053	−0·19450
	ϵ_2	8·29433	−3·94970	3·82076	8·60785	−4·30707	3·33907
	d_4	−0·15738	1·34393	−0·93253	0·35369	−0·27933	0·30349
	d_5	−0·11315	0·28509	0·00222	−0·06785	0·19035	0·01806
$\sigma = 1{\cdot}1$	δ_1	0·29725	−0·66519	0·39580	0·17002	−0·29020	0·14336
	δ_2	2·91846	−4·49967	3·96754	2·47538	−2·26713	1·31600
	ϵ_1	2·86640	−5·47844	4·58321	1·62657	−0·99547	0·53906
	ϵ_2	10·76175	−16·93054	16·82955	9·01488	−7·51176	5·19951
	d_4	−0·07998	1·06268	−0·69006	0·33792	−0·23113	0·25653
	d_5	−0·11873	0·30016	0·01404	−0·04274	0·14184	0·03945
$\sigma = 1{\cdot}2$	δ_1	0·21050	−0·57504	0·40377	0·09625	−0·19681	0·09791
	δ_2	2·77405	−5·14029	4·95087	2·04807	−1·67908	0·98566
	ϵ_1	1·76323	−2·38606	1·86683	1·39437	−0·99977	0·56129
	ϵ_2	8·44204	−11·90013	13·43768	8·79326	−8·48110	5·62015
	d_4	−0·04699	0·96868	−0·64062	0·32262	−0·18271	0·20997
	d_5	−0·10083	0·22512	0·10185	−0·03993	0·14684	0·02954
$\sigma = 1{\cdot}4$	δ_1	0·08390	−0·54290	0·57696	0·07764	0·10186	−0·05721
	δ_2	2·71498	−8·19880	9·30646	0·34742	1·64288	−0·85499
	ϵ_1	1·47271	−4·24209	4·72923	0·03936	1·34936	−0·72213
	ϵ_3	8·06968	−21·08122	26·01889	2·03721	5·11291	−2·00935
	d_4	0·07301	0·52409	−0·25757	0·26233	−0·01163	0·07466
	d_5	−0·11192	0·29721	0·01670	−0·05340	0·20283	−0·01627

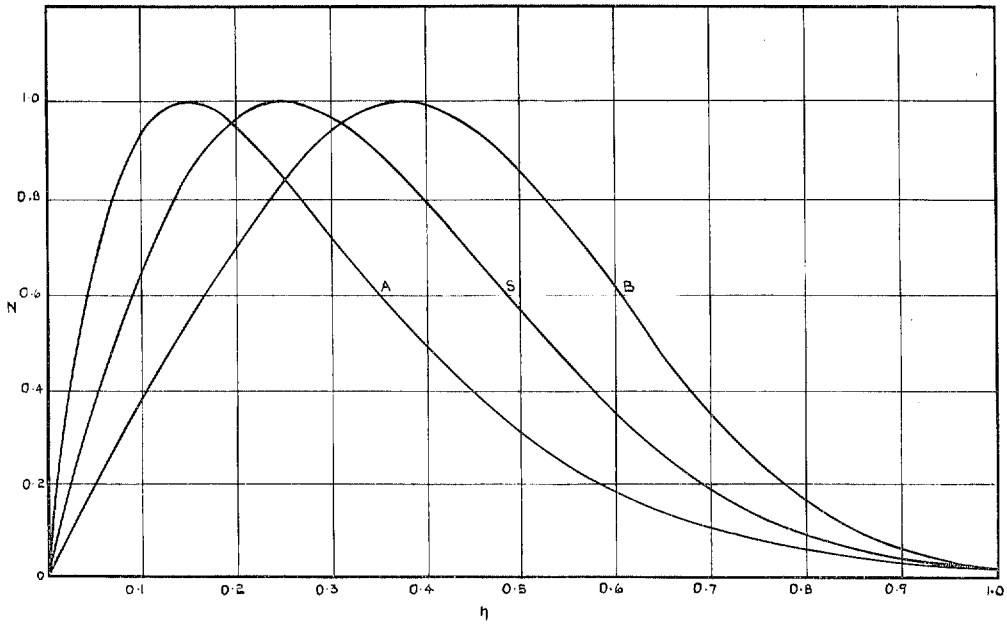

FIG. 1. Basic profiles.

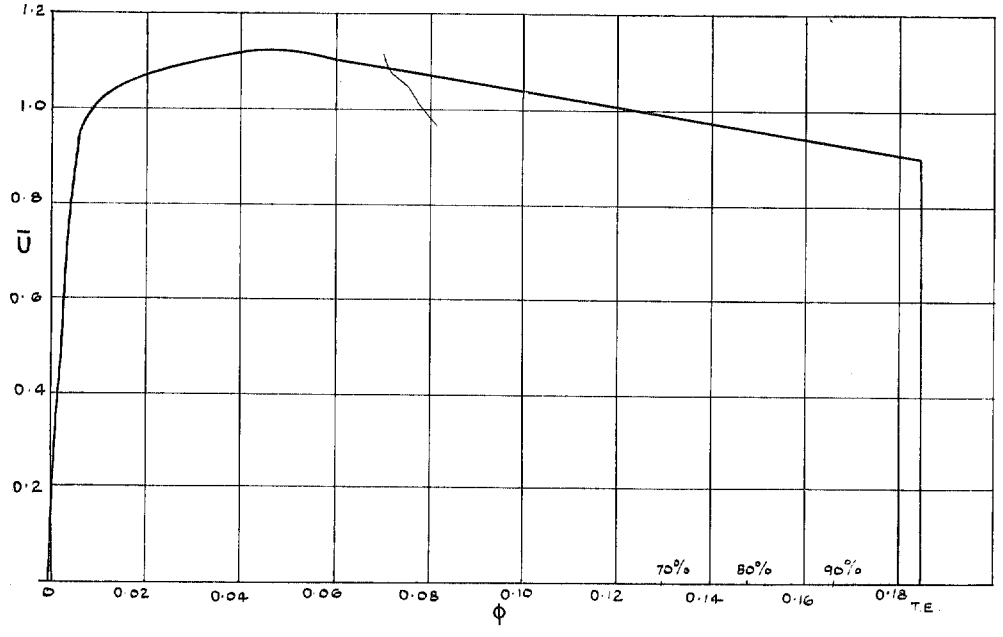

FIG. 2. Velocity distribution, upper surface.

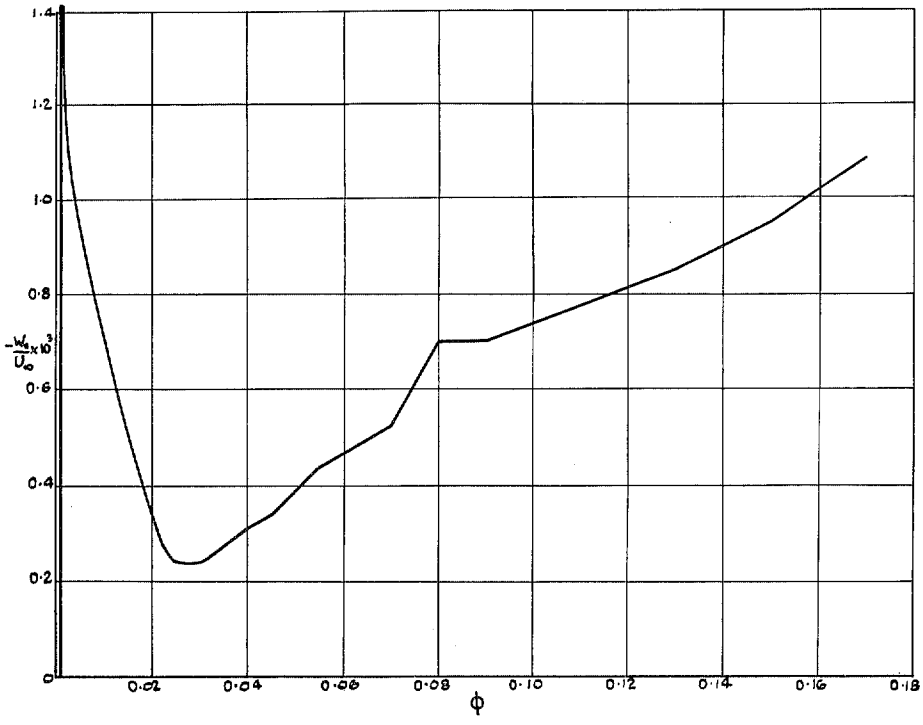

FIG. 3. Suction distribution, upper surface.

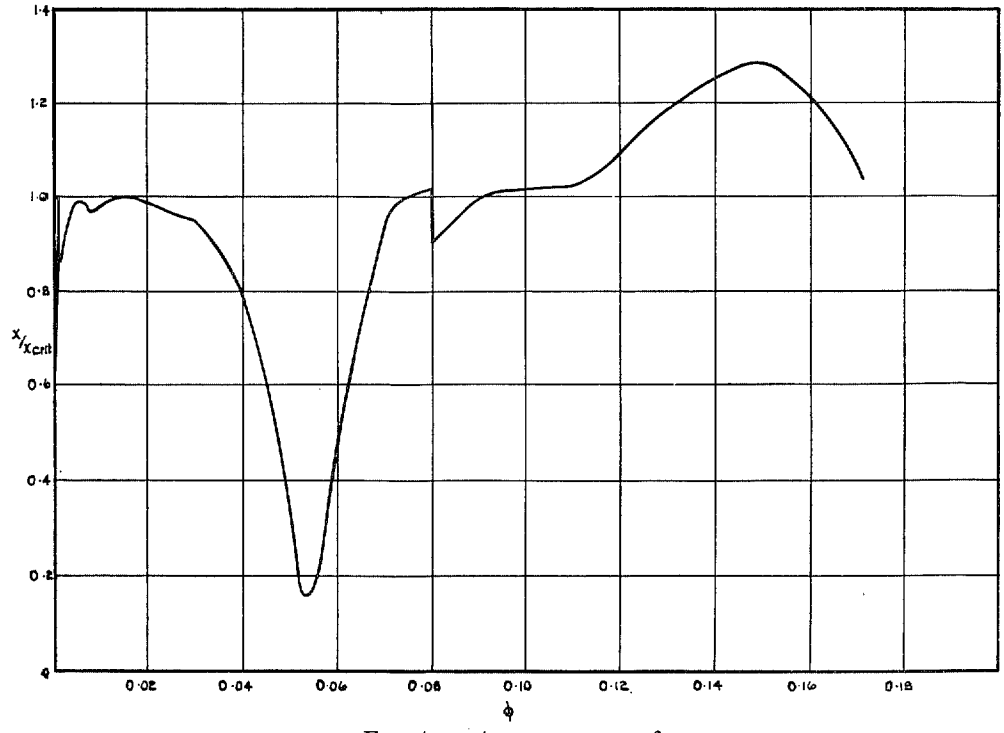

FIG. 4. χ/χ_{crit}, upper surface.

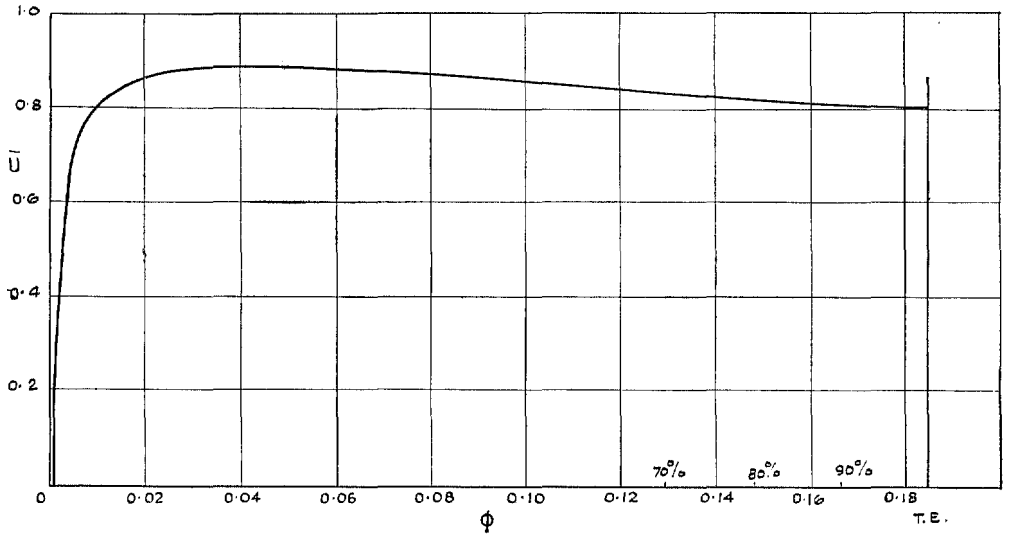

FIG. 5. Velocity distribution, lower surface.

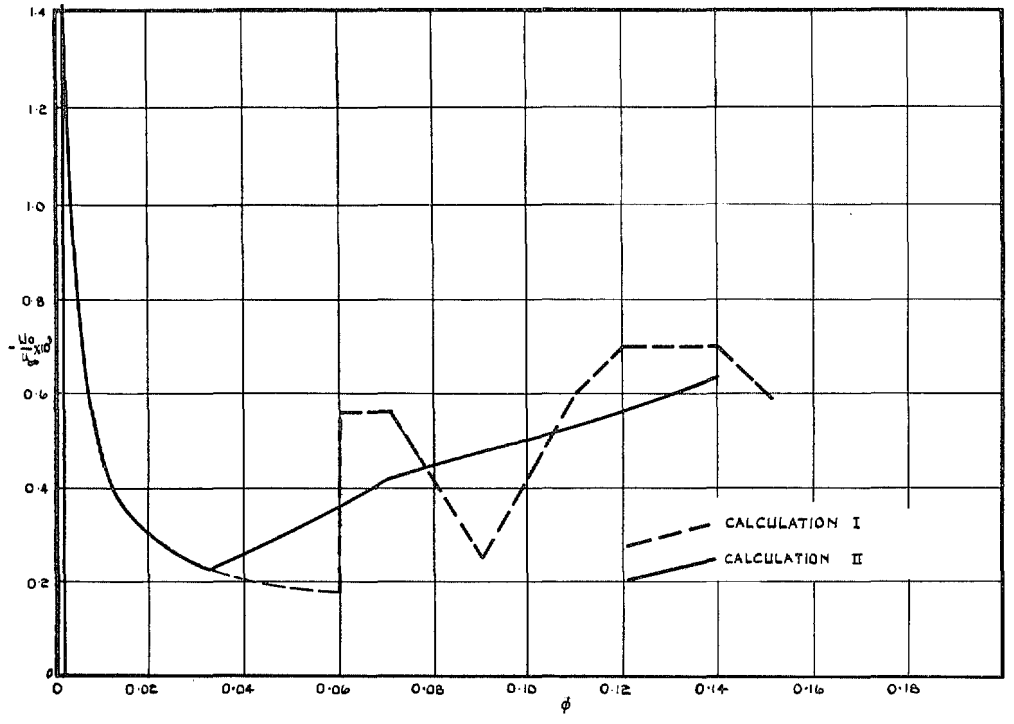

FIG. 6. Suction distributions, lower surface.

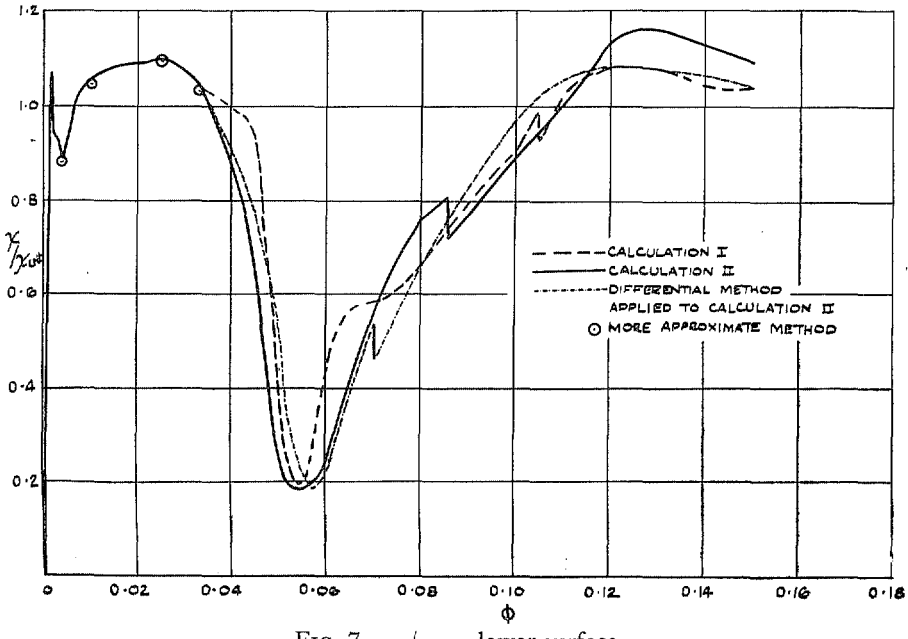

FIG. 7. χ/χ_{crit}, lower surface.

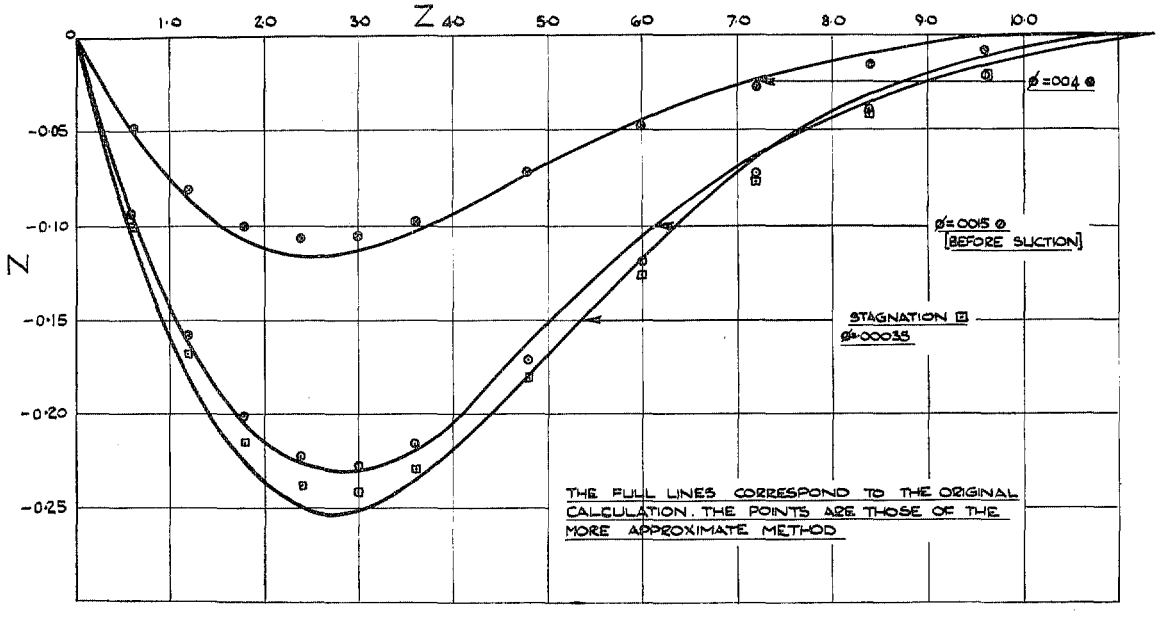

FIG. 8. Comparisons for $\phi = 0{\cdot}00035$ to $\phi = 0{\cdot}004$.

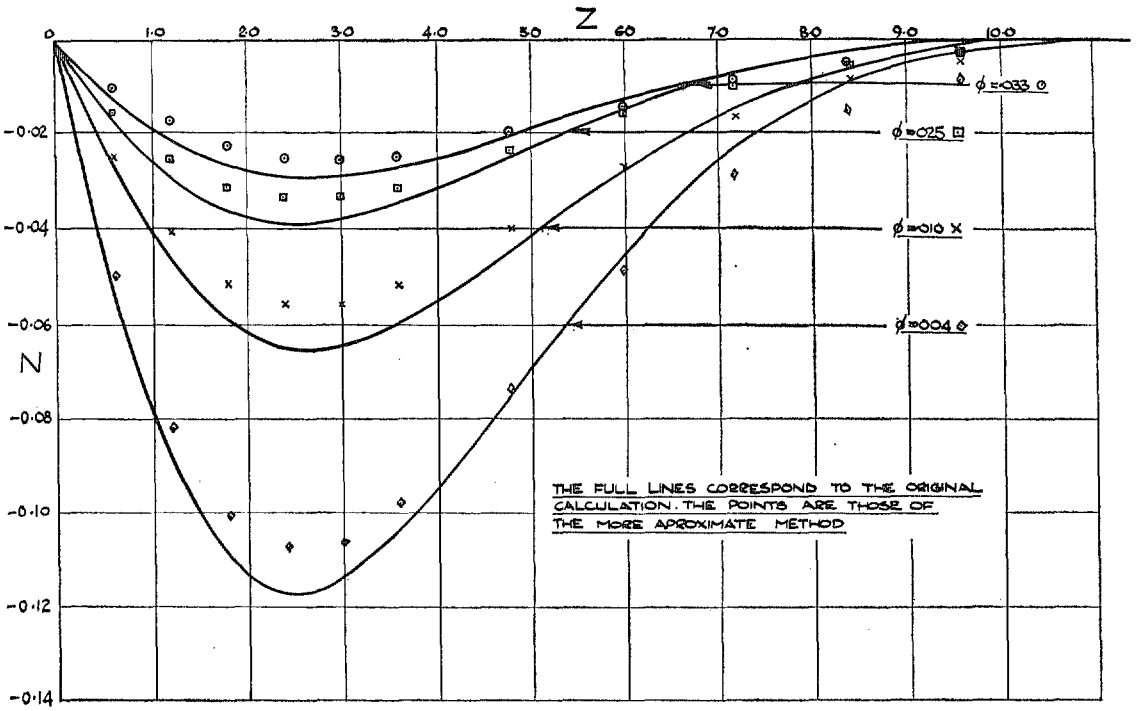

FIG. 9. Comparisons from $\phi = 0{\cdot}004$ to $\phi = 0{\cdot}033$.

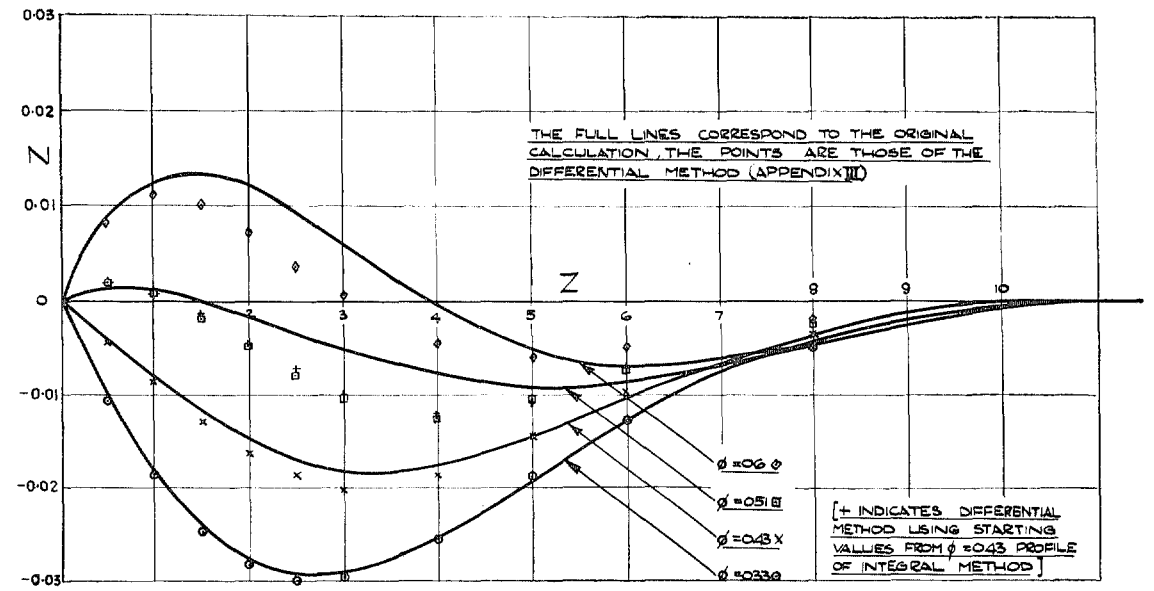

FIG. 10. Comparisons for $\phi = 0{\cdot}033$ to $\phi = 0{\cdot}06$.

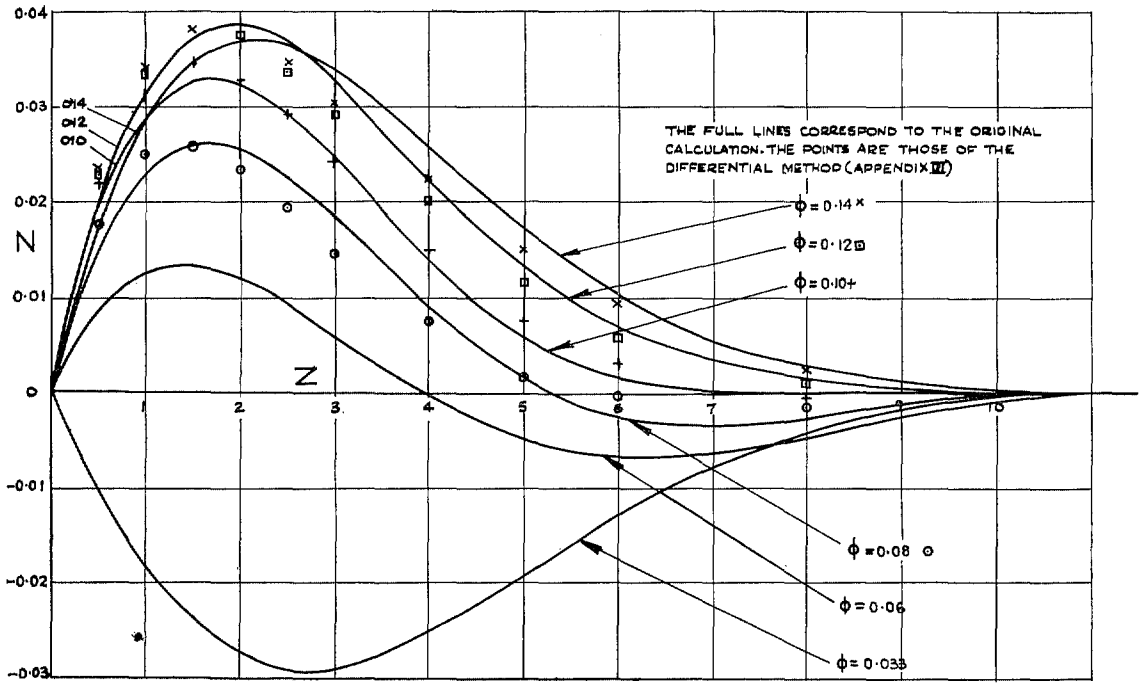

FIG. 11. Comparisons from $\phi = 0{\cdot}08$ to $\phi = 0{\cdot}14$.

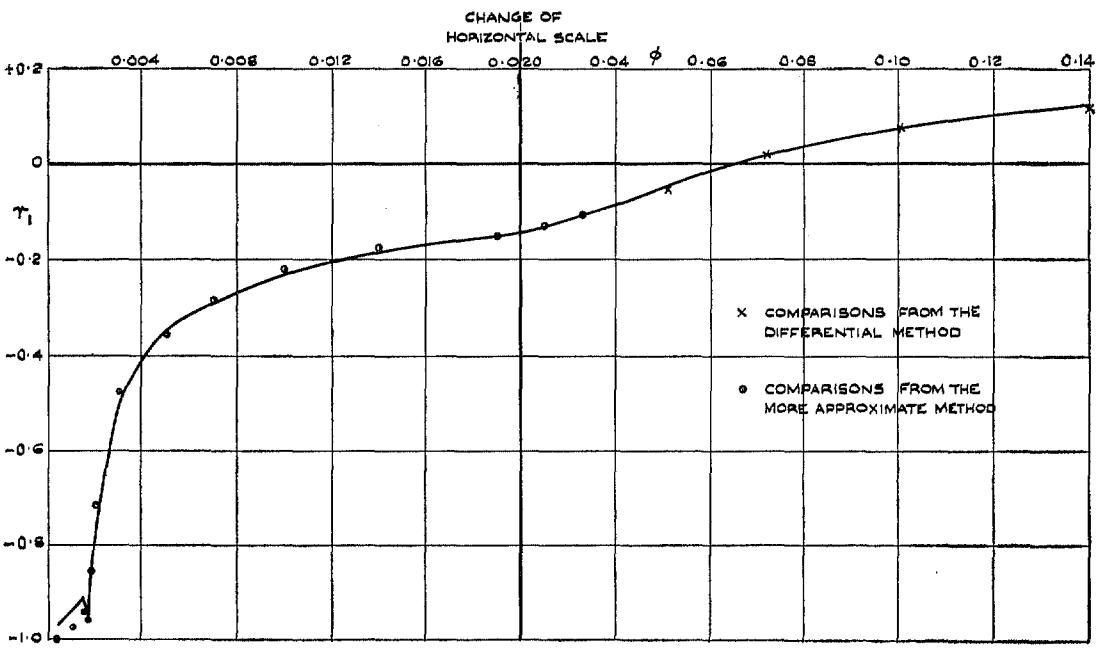

FIG. 12. r_1.

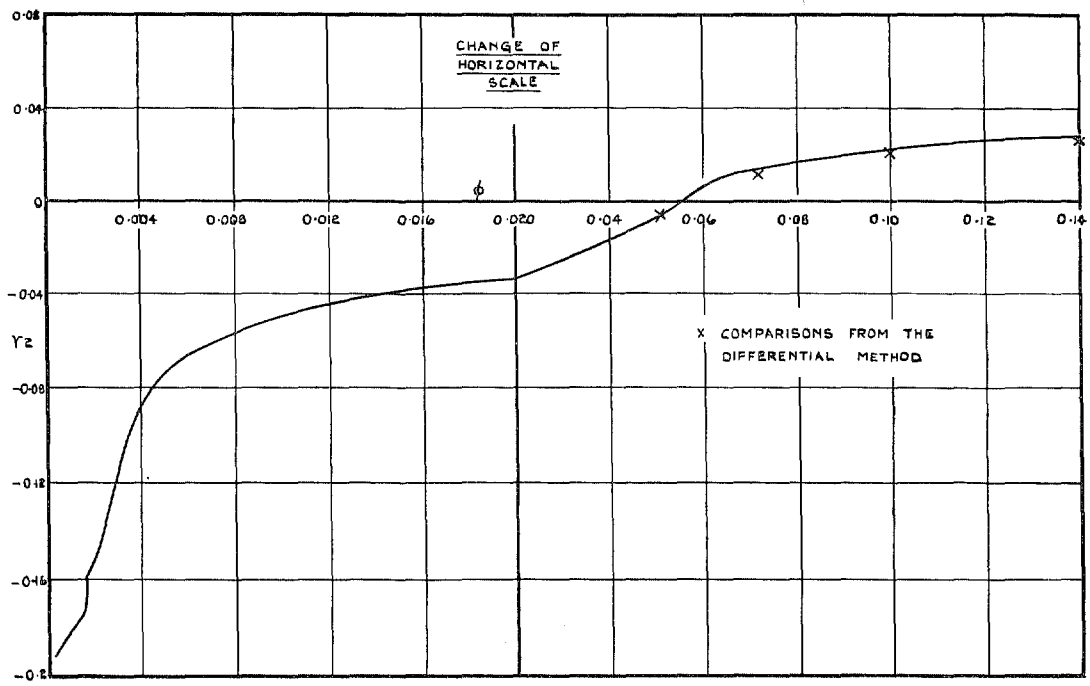

FIG. 13. r_2.

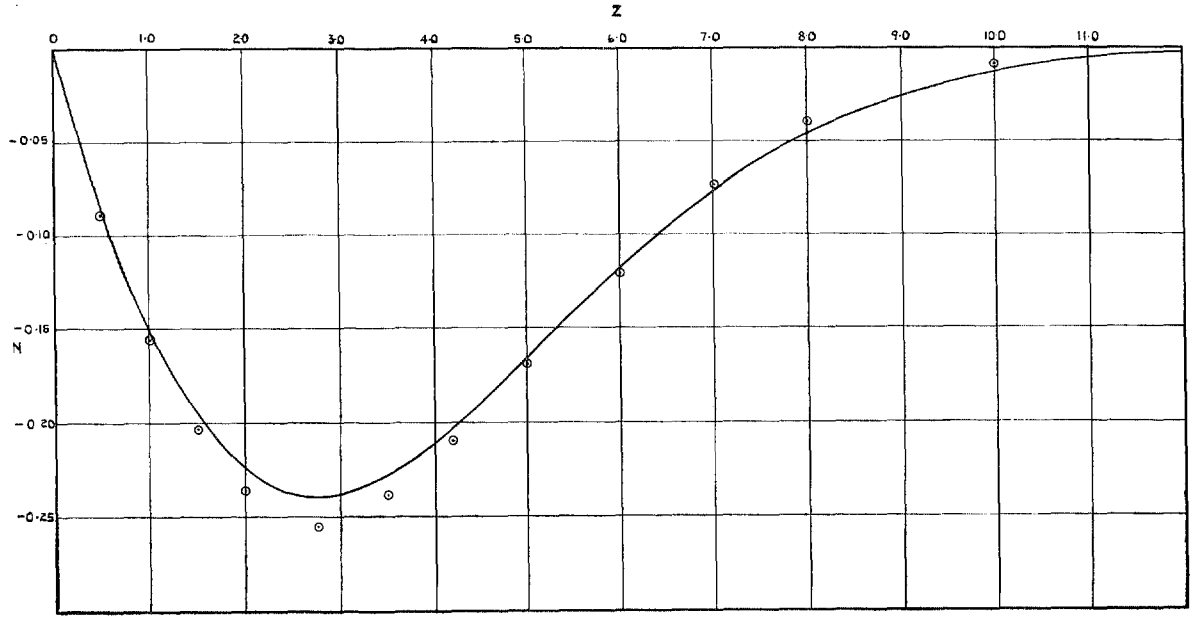

FIG. 14. Stagnation profile. $p = 1$, $K = 0$.

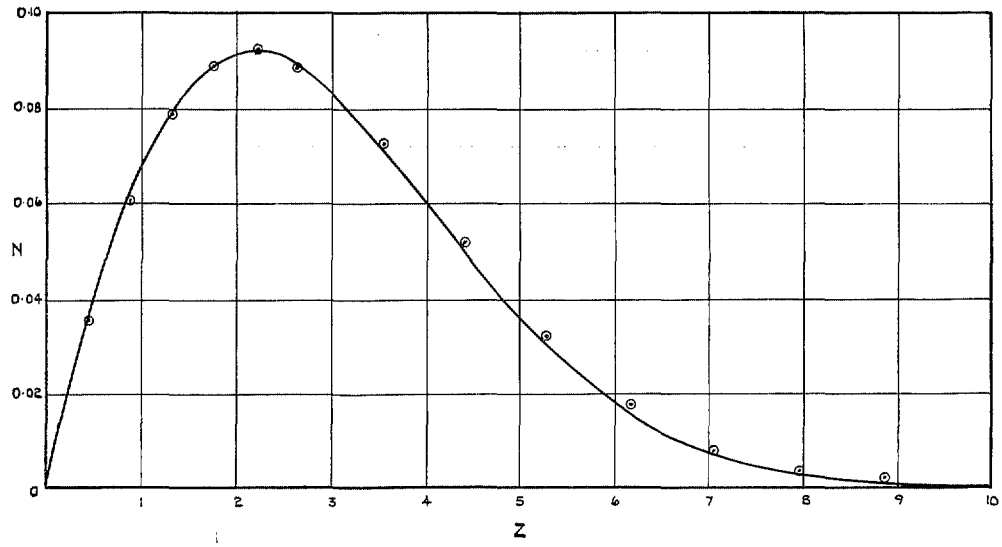

FIG. 15. Similar solution. $p = -1/11$, $K = 0{\cdot}4$.

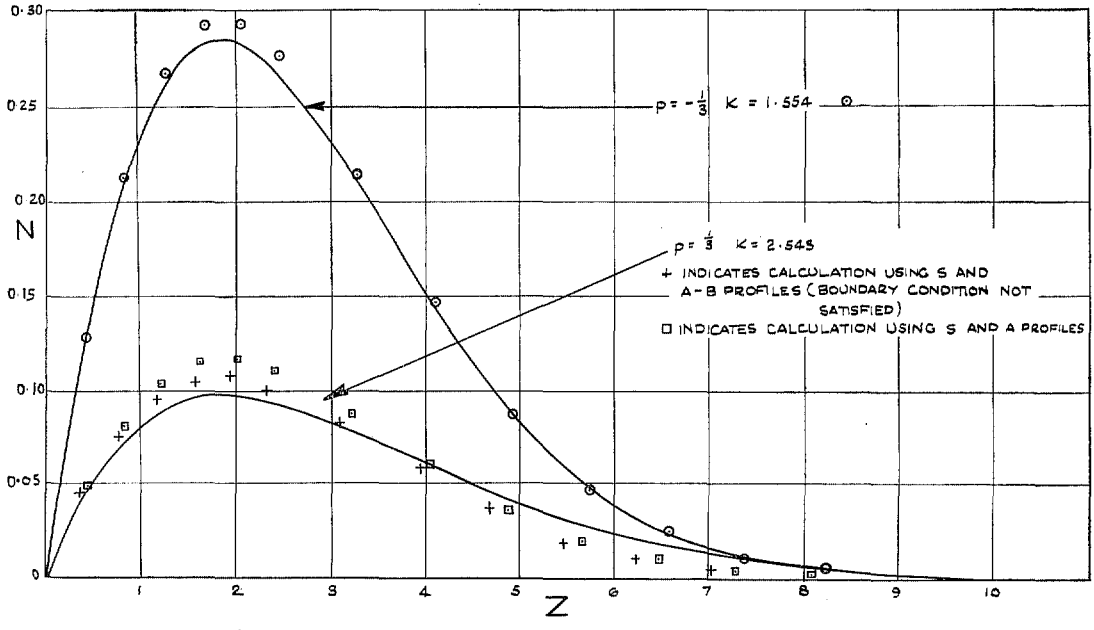

FIG. 16. Similar solutions.

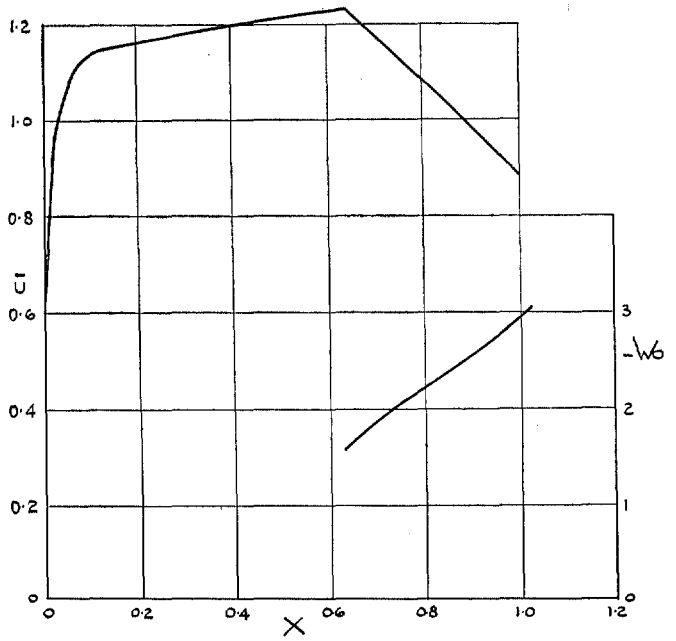

FIG. 17. Velocity and Suction Distributions.

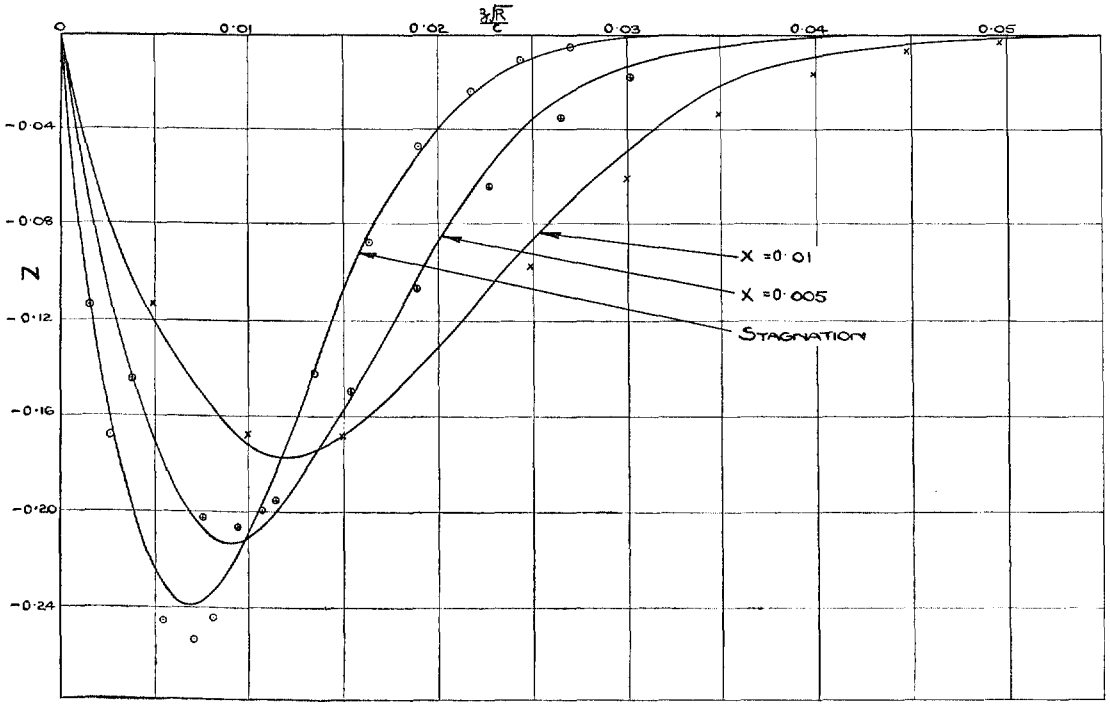

FIG. 18. Comparisons $X = 0$ to $X = 0{\cdot}01$.

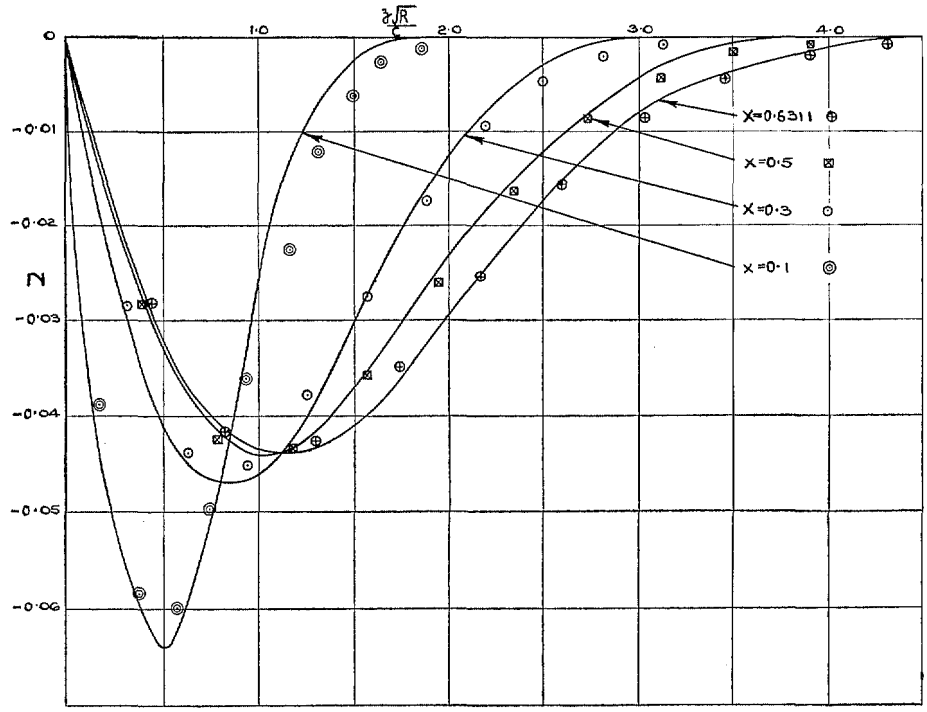

FIG. 19. Comparisons $X = 0{\cdot}1$ to $X = 0{\cdot}6311$.

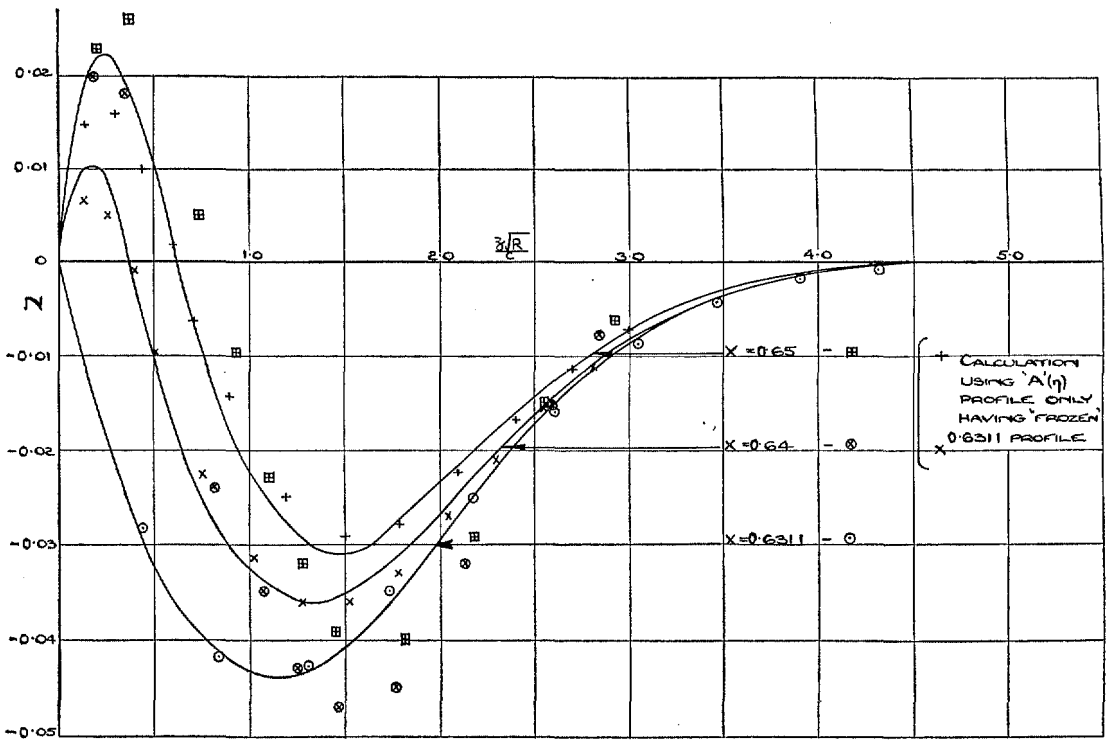

FIG. 20. Comparisons $X = 0{\cdot}6311$ to $X = 0{\cdot}65$.

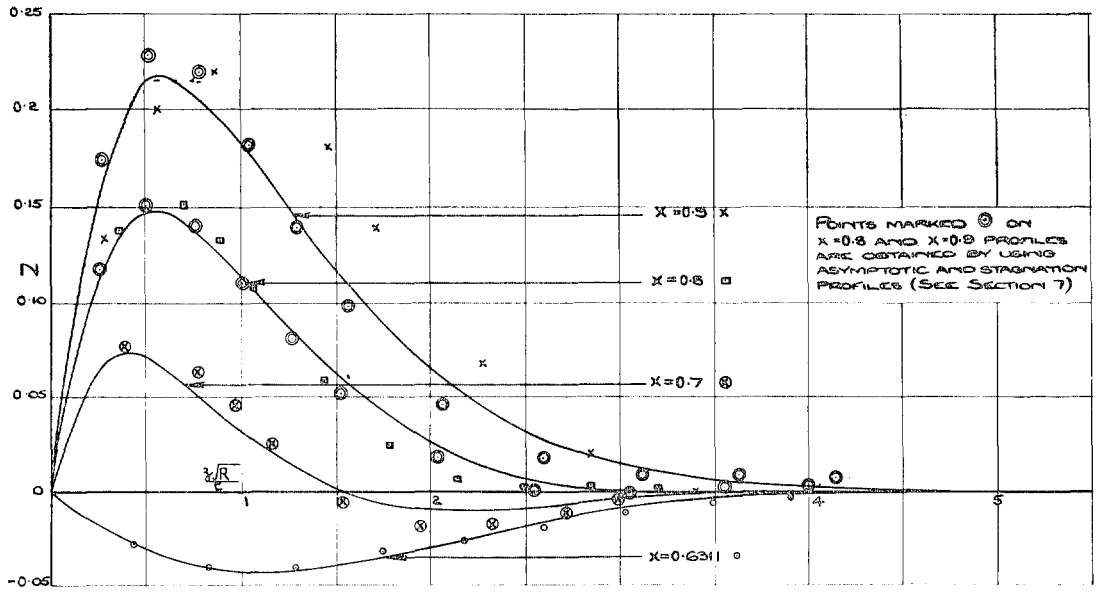

FIG. 21. Comparisons $X = 0{\cdot}6311$ to $X = 0{\cdot}9$.

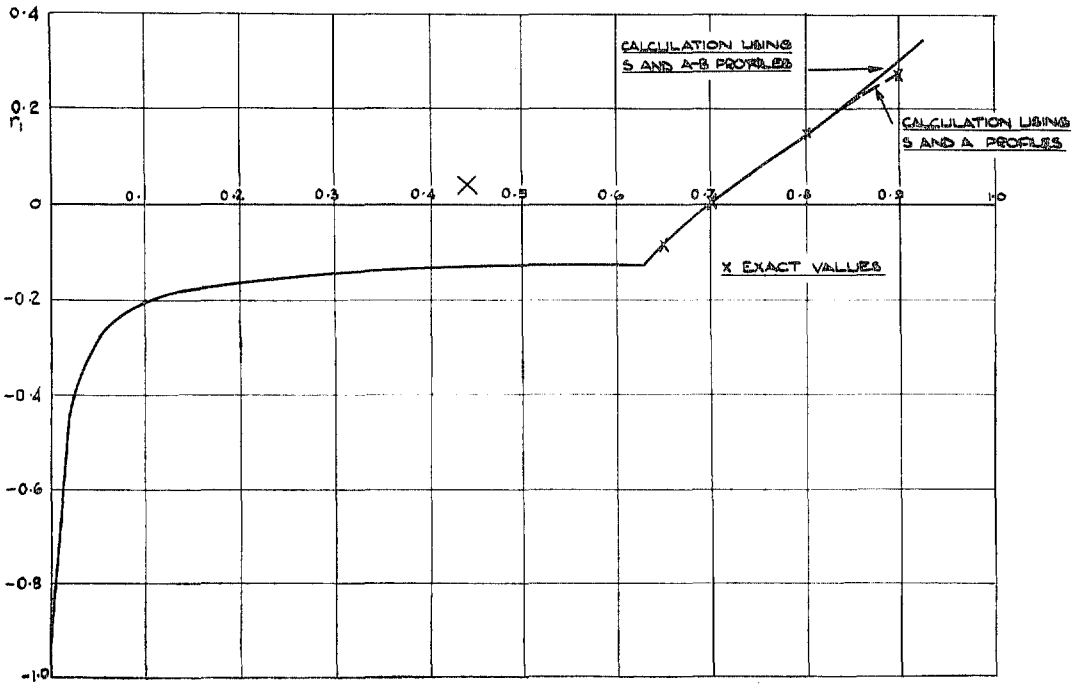

FIG. 22. r_1.

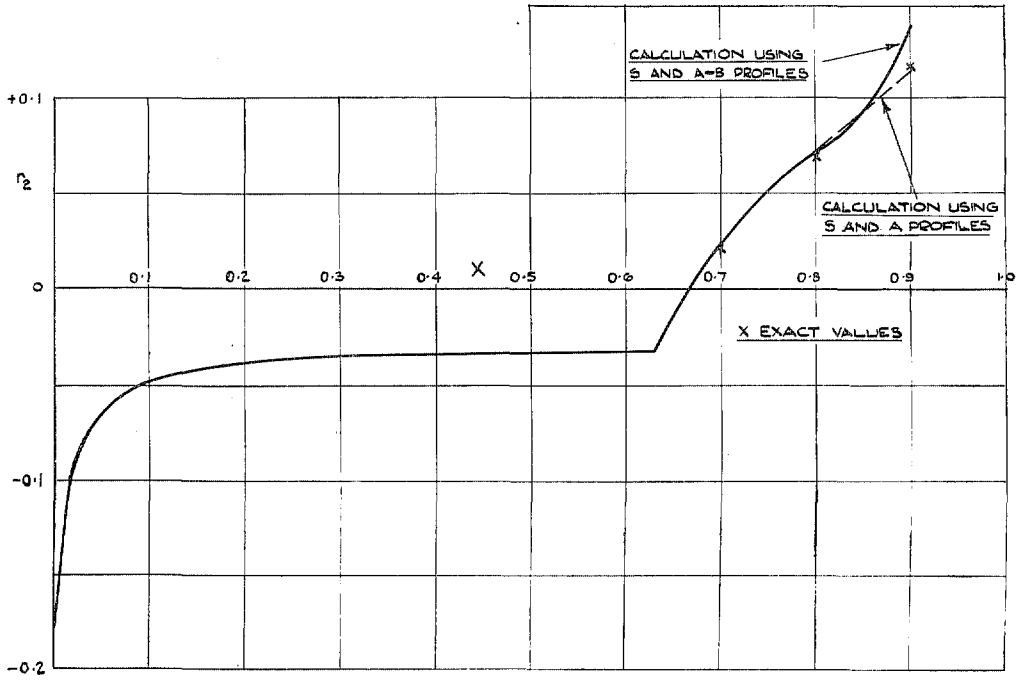

FIG. 23. r_2.

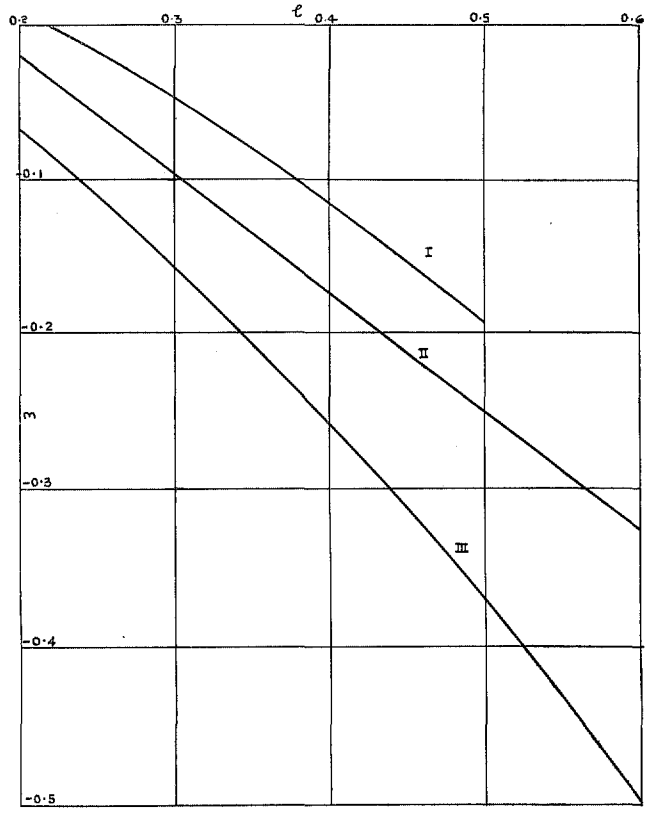

FIG. 24. Lines in l, m, plane.

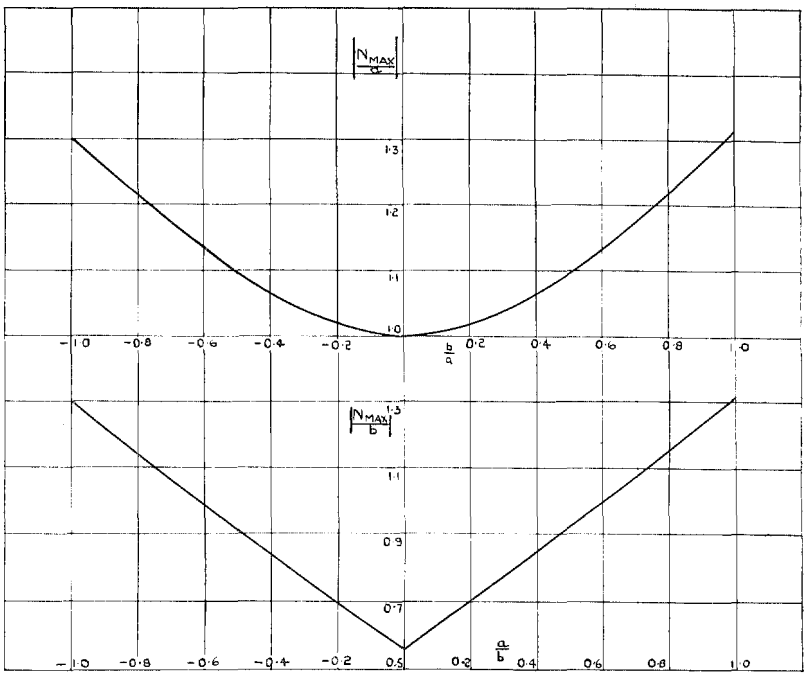

FIG. 25. Chart for determining value of $|N_{\max}|$ from a and b.

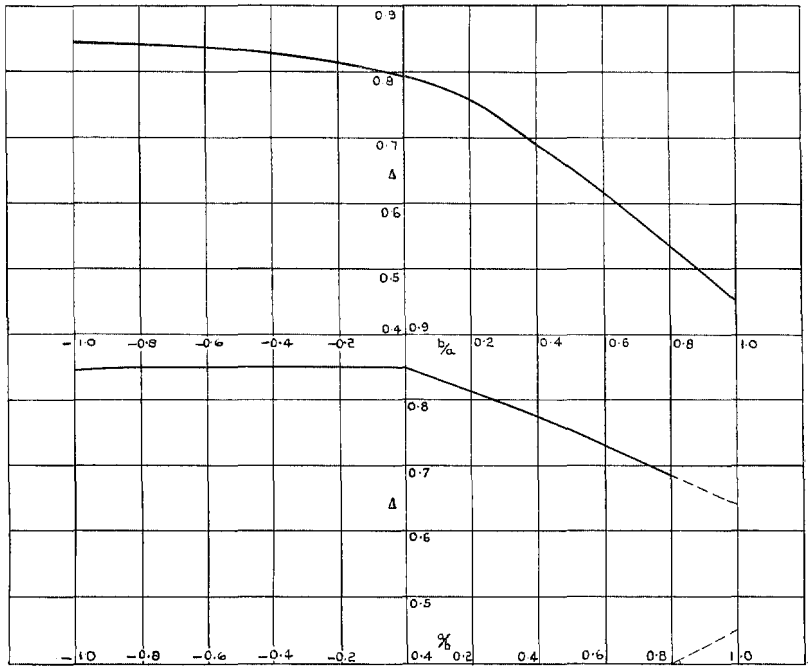

FIG. 26. Chart for determining value of Δ from a and b.

(83324) Wt. 67/1876 K.5 3/62 Hw.

Publications of the Aeronautical Research Council

ANNUAL TECHNICAL REPORTS OF THE AERONAUTICAL RESEARCH COUNCIL (BOUND VOLUMES)

1941 Aero and Hydrodynamics, Aerofoils, Airscrews, Engines, Flutter, Stability and Control, Structures. 63*s.* (post 2*s.* 3*d.*)

1942 Vol. I. Aero and Hydrodynamics, Aerofoils, Airscrews, Engines. 75*s.* (post 2*s.* 3*d.*)
Vol. II. Noise, Parachutes, Stability and Control, Structures, Vibration, Wind Tunnels. 47*s.* 6*d.* (post 1*s.* 9*d.*)

1943 Vol. I. Aerodynamics, Aerofoils, Airscrews. 80*s.* (post 2*s.*)
Vol. II. Engines, Flutter, Materials, Parachutes, Performance, Stability and Control, Structures. 90*s.* (post 2*s.* 3*d.*)

1944 Vol. I. Aero and Hydrodynamics, Aerofoils, Aircraft, Airscrews, Controls. 84*s.* (post 2*s.* 6*d.*)
Vol. II. Flutter and Vibration, Materials, Miscellaneous, Navigation, Parachutes, Performance, Plates and Panels, Stability, Structures, Test Equipment, Wind Tunnels. 84*s.* (post 2*s.* 6*d.*)

1945 Vol. I. Aero and Hydrodynamics, Aerofoils. 130*s.* (post 3*s.*)
Vol. II. Aircraft, Airscrews, Controls. 130*s.* (post 3*s.*)
Vol. III. Flutter and Vibration, Instruments, Miscellaneous, Parachutes, Plates and Panels, Propulsion. 130*s.* (post 2*s.* 9*d.*)
Vol. IV. Stability, Structures, Wind Tunnels, Wind Tunnel Technique. 130*s.* (post 2*s.* 9*d.*)

1946 Vol. I. Accidents, Aerodynamics, Aerofoils and Hydrofoils. 168*s.* (post 3*s.* 3*d.*)
Vol. II. Airscrews, Cabin Cooling, Chemical Hazards, Controls, Flames, Flutter, Helicopters, Instruments and Instrumentation, Interference, Jets, Miscellaneous, Parachutes. 168*s.* (post 2*s.* 9*d.*)
Vol. III. Performance, Propulsion, Seaplanes, Stability, Structures, Wind Tunnels. 168*s.* (post 3*s.*)

1947 Vol. I. Aerodynamics, Aerofoils, Aircraft. 168*s.* (post 3*s.* 3*d.*)
Vol. II. Airscrews and Rotors, Controls, Flutter, Materials, Miscellaneous, Parachutes, Propulsion, Seaplanes, Stability, Structures, Take-off and Landing. 168*s.* (post 3*s.* 3*d.*)

Special Volumes

Vol. I. Aero and Hydrodynamics, Aerofoils, Controls, Flutter, Kites, Parachutes, Performance, Propulsion, Stability. 126*s.* (post 2*s.* 6*d.*)
Vol. II. Aero and Hydrodynamics, Aerofoils, Airscrews, Controls, Flutter, Materials, Miscellaneous, Parachutes, Propulsion, Stability, Structures. 147*s.* (post 2*s.* 6*d.*)
Vol. III. Aero and Hydrodynamics, Aerofoils, Airscrews, Controls, Flutter, Kites, Miscellaneous, Parachutes, Propulsion, Seaplanes, Stability, Structures, Test Equipment. 189*s.* (post 3*s.* 3*d.*)

Reviews of the Aeronautical Research Council

1939–48 3*s.* (post 5*d.*) 1949–54 5*s.* (post 5*d.*)

Index to all Reports and Memoranda published in the Annual Technical Reports

1909–1947 R. & M. 2600 6*s.* (post 2*d.*)

Indexes to the Reports and Memoranda of the Aeronautical Research Council

Between Nos. 2351–2449	R. & M. No. 2450	2*s.* (post 2*d.*)
Between Nos. 2451–2549	R. & M. No. 2550	2*s.* 6*d.* (post 2*d.*)
Between Nos. 2551–2649	R. & M. No. 2650	2*s.* 6*d.* (post 2*d.*)
Between Nos. 2651–2749	R. & M. No. 2750	2*s.* 6*d.* (post 2*d.*)
Between Nos. 2751–2849	R. & M. No. 2850	2*s.* 6*d.* (post 2*d.*)
Between Nos. 2851–2949	R. & M. No. 2950	3*s.* (post 2*d.*)
Between Nos. 2951–3049	R. & M. No. 3050	3*s.* 6*d.* (post 2*d.*)

HER MAJESTY'S STATIONERY OFFICE

from the addresses overleaf

Printed and published by
HER MAJESTY'S STATIONERY OFFICE

To be purchased from
York House, Kingsway, London W.C.2
423 Oxford Street, London W.1
13A Castle Street, Edinburgh 2
109 St. Mary Street, Cardiff
39 King Street, Manchester 2
50 Fairfax Street, Bristol 1
35 Smallbrook, Ringway, Birmingham 5
80 Chichester Street, Belfast 1
or through any bookseller

Printed in England

S.O. Code No. 23-3241